

## Article

# Control Methodologies to Mitigate and Regulate Second-Order Ripples in DC–AC Conversions and Microgrids: A Brief Review

Shivam Chaturvedi <sup>1</sup>, Mengqi Wang <sup>1,\*</sup>, Yaoyu Fan <sup>1</sup>, Deepak Fulwani <sup>2</sup>, Guilherme Vieira Hollweg <sup>1</sup>, Shahid Aziz Khan <sup>1</sup> and Wencong Su <sup>1</sup>

<sup>1</sup> Department of Electrical and Computer Engineering, University of Michigan-Dearborn, Dearborn, MI 48128, USA

<sup>2</sup> Department of Electrical Engineering, Indian Institute of Technology Jodhpur, Jodhpur 342030, India

\* Correspondence: mengqi@umich.edu

**Abstract:** Second-order ripples occur in the voltage and current during any DC–AC power conversion. These conversions occur in the voltage source inverters (VSIs), current source inverters (CSIs), and various single-stage inverters (SSIs) topologies. The second-order ripples lead to oscillating source node currents and DC bus voltages when there is an interconnection between the AC and DC microgrids or when an AC load is connected to the DC bus of the microgrid. Second-order ripples have various detrimental effects on the sources and the battery storage. In the storage battery, they lead to the depletion of electrodes. They also lead to stress in the converter or inverter components. This may lead to the failure of a component and hence affect the reliability of the system. Furthermore, the second-order ripple currents (SRCs) lead to ripple torque in wind turbines and lead to mechanical stress. SRCs cause a rise in the temperature of photovoltaic panels. An increase in the temperature of PV panels leads to a reduction in the power generated. Furthermore, the second-order voltage and current oscillations lead to a varying maximum power point in PV panels. Hence, the maximum power may not be extracted from it. To mitigate SRCs, oversizing of the components is needed. To improve the lifespan of the sources, storage, and converter components, the SRCs must be mitigated or kept within the desired limits. In the literature, different methodologies have been proposed to mitigate and regulate these second-order ripple components. This manuscript presents a comprehensive review of different effects of second-order ripples on different sources and the methodologies adopted to mitigate the ripples. Different active power decoupling methodologies, virtual impedance-based methodologies, pulse width modulation-based signal injection methodologies, and control methods adopted in distributed power generation methods for DC microgrids have been presented. The application of ripple control methods spans from single converters such as SSIs and VSIs to a network of interconnected converters. Furthermore, different challenges in the field of virtual impedance control and ripple mitigation in distributed power generation environments are discussed. This paper brings a review regarding control methodologies to mitigate and regulate second-order ripples in DC–AC conversions and microgrids.

**Keywords:** power decoupling; virtual resistance; virtual impedance; single-stage inverters; qSBI; eqSBI; qZSI



**Citation:** Chaturvedi, S.; Wang, M.; Fan, F.; Fulwani, D.; Hollweg, G.V.; Khan, S.A.; Su, W. Control Methodologies to Mitigate and Regulate Second-Order Ripples in DC–AC Conversions and Microgrids: A Brief Review. *Energies* **2023**, *16*, 817. <https://doi.org/10.3390/en16020817>

Academic Editor: José Matas

Received: 12 November 2022

Revised: 28 December 2022

Accepted: 4 January 2023

Published: 10 January 2023



**Copyright:** © 2023 by the authors. Licensee MDPI, Basel, Switzerland. This article is an open access article distributed under the terms and conditions of the Creative Commons Attribution (CC BY) license (<https://creativecommons.org/licenses/by/4.0/>).

## 1. Introduction

The second-order ripples occur during any DC–AC power conversion, AC–DC power conversion, unbalanced three-phase system and multi-stage converters. These ripples can be observed in the DC side voltages and the currents. The oscillations occur at twice the AC side frequency. Let us analyze the ripple in a DC–AC conversion. The output power of all the DC–AC conversion topologies consists of a constant component and a pulsating component. The constant component depends on the power factor of the load connected

at the output terminals, while the pulsating component oscillates at twice the inverter output supply frequency. The output power of an inverter  $P_{ac} = V_{ac} I_{ac}$  at a particular time instance as,

$$P_{ac} = V_{ac} I_{ac} = V_m \cos(\omega t) I_m \cos(\omega t - \phi). \quad (1)$$

Decompose the above equation to obtain the DC component  $P_c$  of the output power and the ripple component  $P_r$  of the output power:

$$P_{ac} = \frac{1}{2} V_m I_m \cos(\phi) + \frac{1}{2} V_m I_m \cos(2\omega t - \phi) = P_c + P_r, \quad (2)$$

where  $\omega$  is the supply frequency of the AC load;  $\phi$  is the load power factor angle; and  $I_m$  and  $V_m$  are the maximum amplitude of the current and the voltage, respectively. As can be observed from (2), the ripple component of power  $P_r$  oscillates at twice the AC supply frequency (where  $\omega$  is the AC supply frequency). This component is responsible for the voltage and source-current oscillations. The pulsating power at the inverter output terminals leads to the reflection of the second-order harmonics at the DC end. This pulsating component leads to oscillations in voltage and currents at the DC side. In DC-AC conversions, the second-order harmonics are observed primarily in the source current, as the source voltage is nearly constant. In two-stage DC-DC-AC conversion, the oscillations occur in the terminal capacitor voltage. The ripple currents also propagate through the intermediate boost converter to the source. In SSIs, the DC-AC conversion takes place during the non-shoot-through time interval. During this stage, the power is delivered to the load. Hence, the second-order ripples propagate through the impedance network of the SSIs to the source. These ripples have various detrimental affects on the sources such as PV, wind turbines, energy storage and converter components. It leads to the heating of components and reduction of its life span. The second-order voltage and current oscillations lead to varying maximum power points in PV panels. Hence, the maximum power may not be extracted from it. To mitigate the SRCs, oversizing of the components is needed. In terms of batteries, the SRCs cause the depletion of electrodes when drawn beyond a certain limit for a long time. It also causes a rise in battery temperature. To improve the lifespan of the sources, battery storage, and converter components, the SRCs must be mitigated or kept within the desired limits. In the literature, different active and passive methods have been proposed to mitigate, reduce, or share the ripple component. Different virtual impedance-based methods are also being used which have the benefit of ripple reduction without the addition of any extra added component. The ripple currents can also be distributed among the sources as per their capability by regulating the impedance using the virtual control methods. This review article spans all the methodologies adopted with respect to different applications ranging from DC-DC-AC converters to DC-AC inverters, rectifiers, three-phase converters, single-stage inverters, and microgrids. In an environment such as a DC microgrid, these SRCs become distributed among the network depending on the output impedance of the interfacing converter when seen from the DC bus side.

A two-node network without any droop or virtual impedance is shown in Figure 1a. A converter that has low impedance has to bear more SRCs compared with converters with high impedance. Hence, in Figure 1, if  $Z_1 > Z_2$ , the SRC in the second node will be higher. The constant power demand is shared as per the line resistance values. Furthermore, the interconnecting line resistances also affect the SRC distribution. The SRCs propagate to the source in the absence of any SRC mitigation circuitry. The ripple and proportional sharing is regulated virtually by varying the droop  $R_d$  and virtual impedance magnitudes  $Z_v$ , as shown in Figure 1b. The manuscript presents a brief review of different methodologies adopted to mitigate second-order ripples in single DC-AC, DC-DC, single-stage inverters, and distributed microgrids. The contributions of the manuscript are as follows:

- Discuss different active and passive control methods implemented to mitigate the second-order ripples in voltage and source currents.

- Present different virtual impedance control and PWM-based methodologies to mitigation and regulate second-order ripples in DC–AC power converters and single-stage inverters.
- Present control methodologies adopted in distributed power generation systems such as a DC microgrid to manage the ripple distribution among the sources.
- Present and discuss the issues due to the integration of a ripple control loop with the primary and secondary control levels in the microgrid.

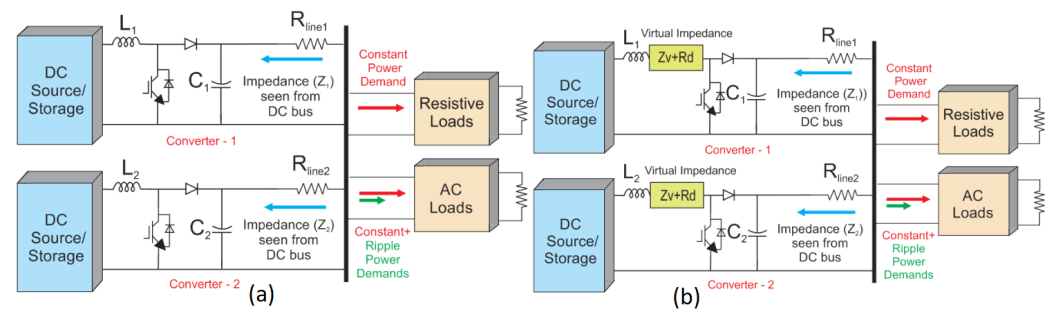


**Figure 1.** Impedance of node in microgrid (a) Without droop and virtual impedance  $Z_v$ . (b) With droop  $R_d$  and  $Z_v$ , if the  $Z_1 > Z_2$  ripple in node-2 will be more. This is regulated using  $R_d$  and  $Z_v$  virtually.

## 2. Need for Power Conversion

Power generation, distribution, and consumption consist of different types of sources, distribution strategies, and loads. The power generation consists of traditional renewable and non-renewable sources. Sources with synchronous generators generate sinusoidal voltages, while those with photovoltaic panels consist of DC output voltages. In this way, many different power sources need power electronics and the control of DC–AC conversion for proper integration with the grid [1–6]. In terms of transmission, high-voltage DC transmission is preferred due to reduced transmission losses [7,8]. This may require AC–DC conversion if the source produces a sinusoidal voltage. Toward the load side, the consumer has loads that can be both AC and DC in nature. Hence, the conversion of DC–AC or vice versa is inevitable. Recently, there has been increased research in the field of grid integration with DC microgrids [9–12]. The integration of a microgrid with the conventional grid requires DC–AC conversion. The DC microgrid is also projected as a traditional grid support system. This means that the power generated by the microgrids is fed to the conventional grid system so as to ensure an uninterrupted power supply to the load centers.

Considering the recent advances in renewable energy research in recent years due to greater environmental concern, there is also a greater demand for power converters that integrate DC–AC conversion [13–15]. In the literature, different topologies are used for DC–AC conversions. Inverter topologies such as voltage source inverters (VSIs) [16–18] and current source inverters (CSIs) [19–21] are used to feed the AC load. In order to achieve a higher AC output, two-stage DC–DC–AC inverter topologies are used [22,23]. These consist of an intermediate boost converter to step up the DC voltage to some desired voltage level. In order to reduce the component count, single-stage inverters are also used to achieve a higher output AC voltage. They incorporate a shoot-through stage in which all the inverter switches are shorted [24,25]. Single-stage inverters have found applications ranging from nano-grid solar PV micro-inverters to electric vehicles, etc. VSIs, CSIs, or single-stage inverters (SSIs) perform the DC–AC conversion. All of the above discussed topologies lead to the generation of second-order ripples. The effects of SRCs can be categorized as follows.

## 3. Effects of SRCs on the Sources

Second-order ripple currents have various detrimental effects on the sources and the interfacing converter components. The effects of SRCs are categorically explained below:

### 3.1. Fuel Cell

Fuel cells (FCs) are used in distributed power generation. They are considered to be an alternative to the traditional nonrenewable sources of energy. However, FCs have a slower dynamic response. The dynamics of FC stacks do not become affected if the current drawn from them is modulated at high frequency. However, a low-frequency oscillating current leads to an interaction between the current drawn and the electrochemical reaction, as shown in [26]. Usually, the interactions between the ripple current and the proton exchange membrane-based fuel cell are analyzed (PEMFC). The fuel cells have slower dynamics, which further degrades in the presence of SRCs [27]. The interaction of fuel cells with various other power electronic converter topologies is widely studied in the literature [28–30]. In [26], an interaction between the input capacitance and electrical response of PEMFC is analyzed. It shows that a larger value capacitor is required to absorb the oscillations in the current drawn so that the electrical dynamics of the FCs are not affected. An equivalent circuit is derived in [31] to analyze the effect of low-frequency ripples on FCs. The experimental results show a 10% reduction in the power that is available in the case of low-frequency current drawn. To regulate the SRC component, a power management unit (PMU) is proposed in [32]. This unit manages the oscillating power between the inverter-fed AC load and the fuel cell. A hybrid system is proposed in [33]. The system consists of a battery system and a fuel cell as the source. The battery provides power during the peak load and during ripple currents when the AC load is driven from the FCs. A battery management system (BMS) is proposed so as to manage the power flow in different scenarios. Hence, to mitigate the SRCs from propagating to the FCs, an extra system has to be developed such as BMS or PMU. This makes the system more costly and complex.

### 3.2. Battery Storage

Power generation in a microgrid depends on the availability of solar or wind energy. These sources are intermittent in nature. As a result, different types of batteries are used to store the surplus energy. The batteries used are nickel cadmium (Ni-Cd) batteries, lead–acid batteries, valve-regulated lead–acid batteries (VRLA), vented lead–acid batteries (VLA), sodium–sulfur (Na-S) batteries, and lithium ion batteries. Each of these batteries has a different capacity to withstand the ripple current drawn. In [34], an analysis is carried out to analyze the effects of ripple on Li-ion batteries. The effects of SRCs are found to be minimal. Similarly, Ni-Cd batteries are also not adversely affected due to the ripple currents, as the impedance of these batteries remains almost constant in fully charged to discharged conditions, as mentioned in the IEEE-1184 standards [35]. However, these batteries are costlier. Lead–acid batteries such as VRLA and VLA have heating issues when the ripple current is drawn from them. There is a reduction of efficiency, and the battery lifetime degrades when a ripple current is drawn for a longer period of time, as specified in the IEEE-519 standards [36]. Different IEEE standards emphasize limiting the ripple current drawn from the batteries. Some of the standards are: IEEE Std 1188-2005 [37], IEEE 1184-2006 [35], IEEE Std for sizing lead–acid batteries [38], and IEEE Std for Ni–Cd battery sizing [39]. Hence, proper batteries must be selected or a proper SRC level must be maintained so as to ensure minimal damage to battery electrodes and to increase the lifetime of the batteries.

### 3.3. Photovoltaic Panels

SRCs cause the operating temperature of PV panels to rise. Any increase in the temperature leads to a reduction of the efficiency of the panels, as specified in [40]. Furthermore, any oscillations in the voltage and currents lead to improper function of the maximum point extraction algorithm. This further degrades the efficiency of power generation of the PV panels, as shown in [41]. To extract the optimum power from the photovoltaic panels, ripple-based extreme seeking control is proposed in [42]. A ripple correlation control for maximum power extraction is proposed in [43]. Particle swarm optimization (PSO)-based

methodologies have also been used so as to extract maximum power during ripple in currents, as in [44]. The degradation of output power due to SRCs is analyzed in [45]. The SSIs used in the microinverter also suffer from the source second-order ripple current. Comprehensive modeling of an SSI with consideration of the ripple currents is presented in [46]. The variation of impedance of PV panels with voltage ripples is analyzed in [47]. Hence, the presence of ripples in the current drawn from PV panels reduces the efficiency, and various complex algorithms have to be used to extract maximum power. Instead, the ripple current must be prevented from being drawn from it.

### 3.4. Wind Turbines

SHCs when drawn from a wind turbine (WT) lead to ripple torque in the turbine. These ripples in torque lead to mechanical stress in the turbine [48]. There are two types of WTs, vertical and horizontal axis wind turbines (VAWTs and HAWTs), depending on the axes of rotation. The ripple in torque reduces the lifetime of a VAWT compared to the HAWT [49]. However, the ripple in torque can be regulated by the usage of adequate gear ratios [50,51]. Hence, SRCs must be regulated rather than allowing them to propagate to the WTs and cause ripple in the torque.

### 3.5. Other Issues Due to SRCs

SRCs affect the sources drastically and lead to a reduction in the operating lifetime. To mitigate the SRCs, the converter components may be oversized [52]. If the converter is designed without considering SRCs, then it may lead to failure of the equipment. The low-frequency oscillations in voltage and current may lead to stress in the active switches or in the capacitors that are used to absorb the ripple content. The capacitor being the weakest element of any circuit may lead to failure, as shown in [53]. The installation of a non-electrolytic capacitor leads to an increase in the cost of the system. If SRCs are not mitigated, there may be oscillation in the voltage, which leads to the problem of LED flickering. In [54], the authors present a comprehensive study to minimize the capacitor in an AC–DC flyback converter connected to an LED with the aim of reducing the flickering due to SRCs. Similarly, an adaptive control is proposed in [55] to remove the electrolytic capacitor and drive the LEDs using a power-factor correction (PFC) circuit with a bidirectional converter. The SRCs lead to oscillation at the DC terminals of the converter and affect the equipment connected to it, as shown in [56]. This affects the equipment lifetime at the consumer end, and the power quality is also degraded.

SRCs can be regulated by active or passive methodology. In passive methodology, the size of passive components, i.e., inductance and capacitance, is increased so as to vary the impedance as seen from the DC bus. The capacitance size is increased to provide the oscillatory power during the DC–AC conversion. The frequency of second-order ripples is usually low. This implies that a large-size capacitor will be required to mitigate the SRCs. Usually, electrolytic capacitors are used instead of aluminum, ceramic, or film capacitors as the electrolytic capacitors are comparatively cheaper. However, electrolytic capacitors are not reliable and are known to have less life compared with the other components [57]. The inductance of the converter can also be increased to reduce the SRC content. However, this leads to an increased weight of the converter, which might not be desirable. Various active filters are also used with the aim of reducing the capacitance requirements. In distributed power generation, the installation of an active or passive filter will lead to an increase in the component count. This will increase the cost and the maintenance requirements of the system. Instead of using active or passive filters, virtual impedance control methodologies have been used in the literature. These have an advantage over other methodologies as they do not require any extra circuitry or bulky filters. The cost of the system also does not increase. However, using virtual impedance control methodologies may have the effect of degradation of the dynamics of the system if not designed properly.

#### 4. Second-Order Ripple Mitigation Methodologies

In the literature, different methodologies have been proposed to mitigate the SRC propagating through a converter. The SRCs are mitigated by using a capacitor at the DC end. The capacitor provides the ripple power required during DC–AC conversion. However, the capacitor size required increases with the reduction in the SRC frequency value. To reduce the capacitor size, various active control methodologies have been proposed. The SRC control methodologies can be broadly categorized as passive power decoupling methodologies, active power decoupling methodologies, and control-oriented methodologies. The descriptions of the different methodologies are as follows:

##### 4.1. Passive Power Decoupling Methodologies

The passive power decoupling methodologies consist of increasing the size of the capacitors and inductors so as to regulate the SRCs, as mentioned in [58]. However, as the frequency of operation is reduced, the size of the passive component has to be increased, as specified in [59]. This leads to an increase of the weight and size of the converter when the inductor size is increased. On the other hand, an increase in capacitor size increases the cost of the system. The bulkier electrolytic capacitors are needed to minimize the cost and absorb the ripple content. Electrolytic capacitors are not reliable [57]. In [56], the authors derive the minimum capacitance required to mitigate the SRC content. In the literature, different methodologies have been proposed so as to minimize the capacitance requirement. In [60], the authors propose a capacitorless inverter so as to reduce the stress on the circuit components. Electrolytic capacitor elimination is also completed in [61,62]. Hence, there is a need to reduce the capacitor size and improve the reliability of the system. For capacitor size reduction, various active power decoupling strategies proposed in the literature are presented in the next subsection.

##### 4.2. Active Power Decoupling Methodologies

The active power decoupling circuit (APDC) consists of extra circuitry through which the SRC is regulated. The circuit can be connected either in parallel or in series with the DC–AC stage converter. The configurations are shown in Figure 2 and Figure 3, respectively.

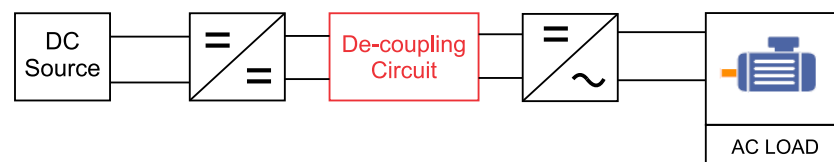


Figure 2. Series interfacing of APDC.

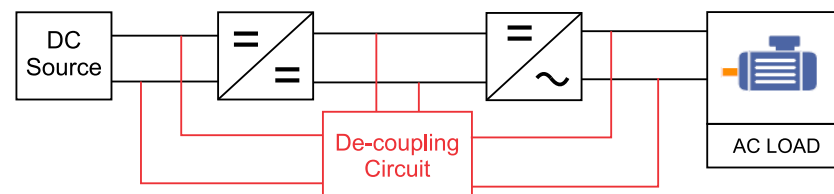


Figure 3. Parallel interfacing of active power APDC.

In [63], the authors propose an active power filter (APF) for the current source inverters (CSIs), as shown in Figure 4. The APF consists of a bidirectional buck–boost converter to store the ripple energy to the passive component of the filter in one half and to provide the ripple energy in the other half. The proposed control leads to considerable mitigation of the voltage and current second-order oscillations. This leads to improved MPPT operations in the PV panels.

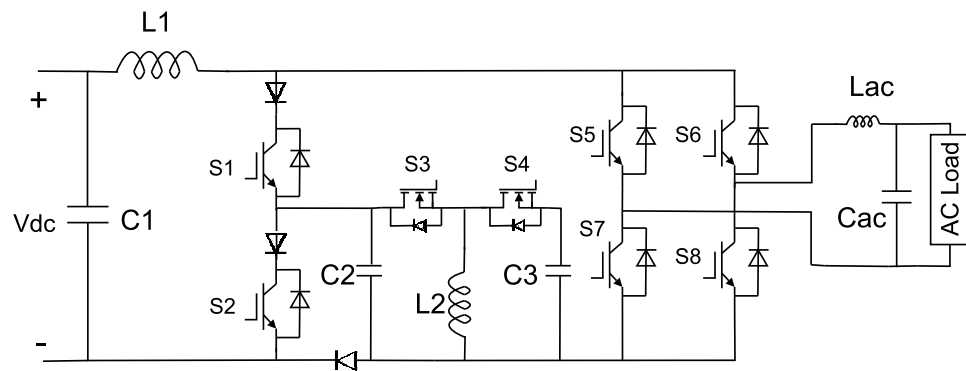


Figure 4. Active power filter for CSIs.

Similarly, an active power buffer circuit is used to store and provide the ripple energy in [64], and a control scheme is also proposed to reduce the second-order ripples while feeding a pure sinusoidal current to the grid interfaced to it. The buffer filter and control is implemented for a CSI. The filter and control were used to obtain 8.9% ripple with THD of 4.2%. A power factor of 99% was obtained with an efficiency of 95%. The implemented active buffer is presented in Figure 5.

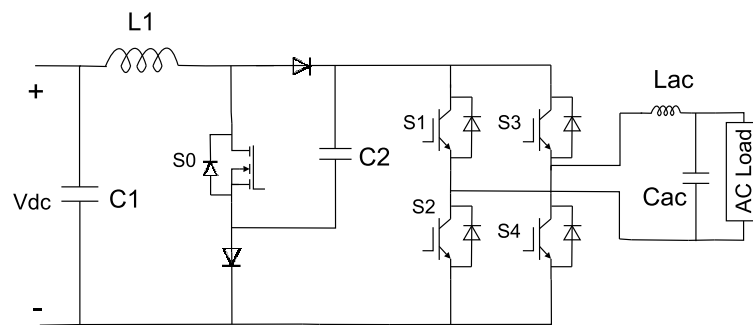


Figure 5. Active power buffer for CSI.

The ripple in the current from the source is reflected on the DC side in a quasi-Z-source inverter (qZSI). To mitigate the ripples, either a bulky capacitor needs to be installed or the size of the impedance network needs to be increased. This leads to an increase in the size and weight of the qZSI. In [65], the authors propose an active filter integrated with the qZSI. The resultant circuit is presented in Figure 6. The low-frequency oscillations are mitigated at the DC end. This will lead to a reduced size of the impedance network. In addition, the size of the capacitor for ripple energy absorption is smaller.

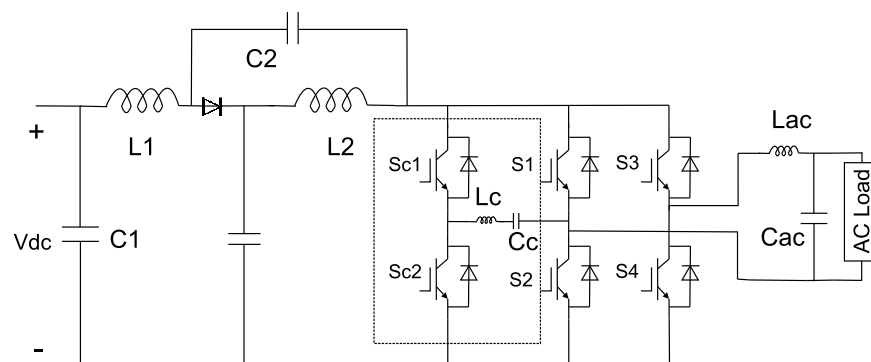
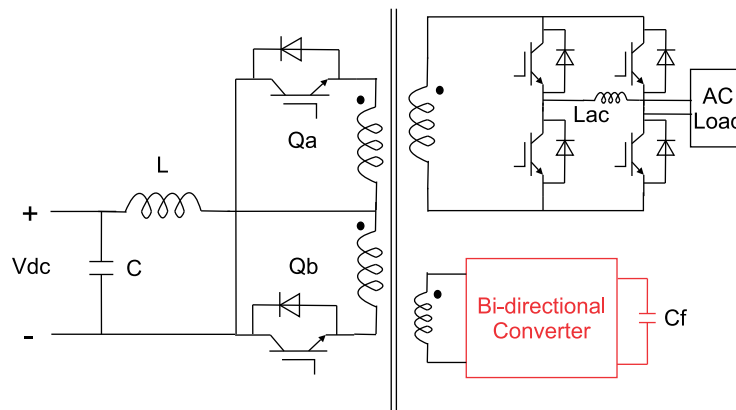


Figure 6. Active filter for qZSIs.

In [56], the ripple current is reduced by considering the ripple energy demand due to the DC–AC conversion. A ripple port is implemented so as to provide the oscillating

second-order power. This approach has the effect of changing the port requirement to a two-quadrant converter, which is formulated with the same switches at the DC end of the inverter, leading to the reduction of converter size and cost. The proposed ripple control configuration is shown in Figure 7.



**Figure 7.** High-frequency flyback based utility interactive topology.

The lifetime of an electrolytic capacitor is reduced due to extreme operating conditions such as high atmospheric temperature. A flyback inverter for PV applications, shown in Figure 8, has been proposed. Capacitor idling methodology is used to derive a circuit topology through a single-ended primary-inductance converter to a two-switch flyback converter. To improve the conversion efficiency, soft switching was implemented. Furthermore, a peak current control was employed to the sinusoidal current to the AC grid interfaced with the converter. A stacked switched capacitor (SCC) architecture is proposed in [66] to improve the energy density of ceramic and film capacitors. The energy density is to be made comparable to the electrolytic capacitors so as to replace them in the system. The SCC architecture can be used as an energy buffer to reduce the power oscillations during the DC–AC conversions. The work has further been extended in [67]. The SCC buffer is enhanced to achieve a high energy density and also high efficiency with the desired DC bus ripples. A bidirectional ripple eliminator is proposed in [68]. The eliminator consists of a bidirectional buck–boost converter with a capacitor as an energy storage element. The voltage of the capacitor terminals can be regulated to be more or less than the DC bus from which the ripples are to be eliminated. This helps in reducing the capacitor requirements in the filter. A rectification system with PFC also consists of the second-order ripples in the DC-side voltage and source currents. In [69], a differential AC–DC rectifier is proposed with inductor current waveform control so as to regulate the ripple content. The usage of electrolytic capacitors is minimized by usage of the proposed control. Another control to compensate for oscillations by putting a voltage source in series with the DC line has been proposed in [70]. This helps in compensating for the DC bus voltage oscillations. A comprehensive analysis of static and dynamic impacts on system characteristics is presented. An active-power decoupling is proposed by using a neural filter. The ripple content in the DC voltage is estimated, and its ratio with the average DC bus is found [71]. This is used to improve the neural SRC filtration method. To improve the system robustness, sliding-mode control is used. In the literature, several authors proposed sliding-mode based techniques for the control of power converters, as [72–77]. To regulate the output impedance of the cascaded converters, an adaptive active capacitor converter (AACC) is proposed in [78]. The AACC acts as the equivalent capacitor and helps to reduce the output impedance of the source converters. This helps to avoid any interaction between the source and load impedance. Similarly, methods to manage output impedance for SRC regulation are proposed in this work.

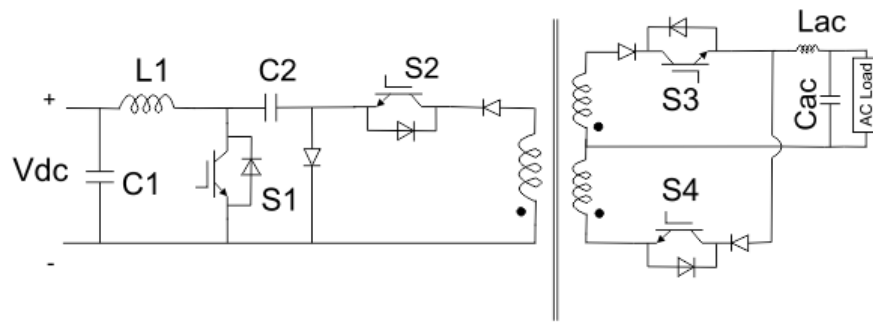


Figure 8. Single-phase PWM voltage source rectifier.

A single-phase pulse width modulation voltage source rectifier capable of feeding a pure sinusoidal current and achieving a zero ripple output current is proposed in [79]. The proposed circuit configuration is shown in Figure 9.

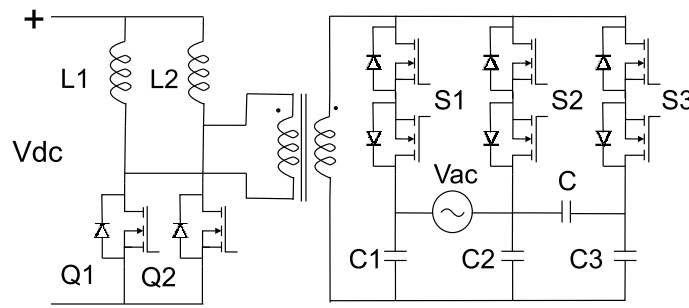


Figure 9. Series interfacing of active power APDC.

Two different control methodologies have been used, which are referred to as the DC-side inductor method and the AC-side inductor method. The proposed control is applicable for storage batteries that are connected to a common DC bus in parallel. An active capacitor reduction circuit (ACRC) is proposed in [80] to minimize the ripple in the DC bus voltage. This facilitates the usage of a smaller-value capacitor to absorb the SRCs. The filter consists of a bidirectional converter controlled by a dual-loop voltage and current control. The proposed ACRC is shown in Figure 10. A buck-based charger is proposed in [81] to provide the charging and filtering capability for electric vehicle application. This helps in reducing the size of the accessories of an EV. Another buck converter-based active power circuitry is proposed in [82].

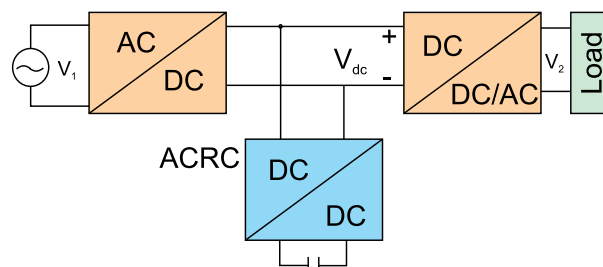
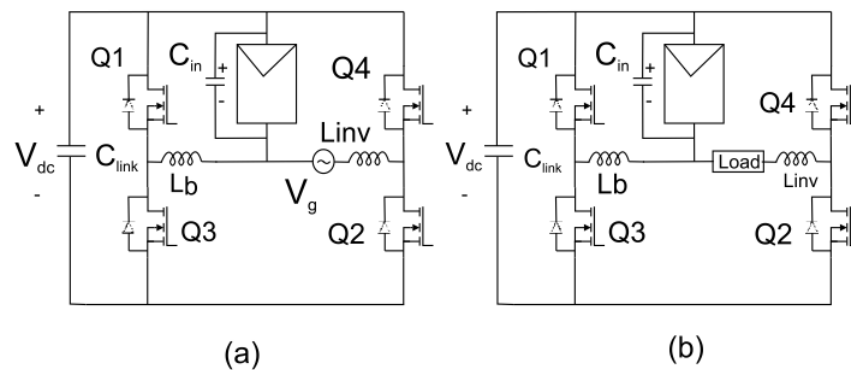


Figure 10. ACRC proposed in [80].

The filter is used for modular multilevel converters (MMCs) [83]. The control configuration reduces the SRCs, and the sub-module capacitor voltage is regulated with a smaller capacitor size. It is applicable for high and medium voltage-level MMCs. A doubly grounded inverter topology is proposed in [84] to eliminate the common mode leakage currents and second-order oscillations in source currents and bus voltages.

The proposed topology is applicable for transformerless PV applications. The configuration eliminates the capacitance coupled with the common ground currents of the inverter. The proposed methodology can be categorized as an active power decoupling scheme. The circuit configuration is presented in Figure 11. A new circuit configuration is proposed in [85] that is capable of power factor correction and power decoupling. The proposed methodology is applied to achieve a DC-side THD as low as 1.5% and ripples of about 6.3%.



**Figure 11.** Doubly grounded inverter topology proposed in [84]: (a) PV connected to the grid. (b) PV connected to the load.

Power factor correction of 99% was achieved with an efficiency of 96%. The control was implemented for a 750 W system. The proposed configuration is shown in Figure 12. An active power decoupling scheme using a dual buck converter and model predictive control is used in [86] to regulate the second-order oscillations. The dual buck converters are controlled to operate at individual cycles. The configuration consists of split capacitors. The proposed ripple regulation configuration is simple and reliable compared with traditional methodologies. In [87], an extra pair of switches is connected at the output of the single phase inverter terminals to confine the ripples to flow through the output capacitors. The proposed configuration provides sinusoidal power with ripple-free DC at the inverter input terminals.

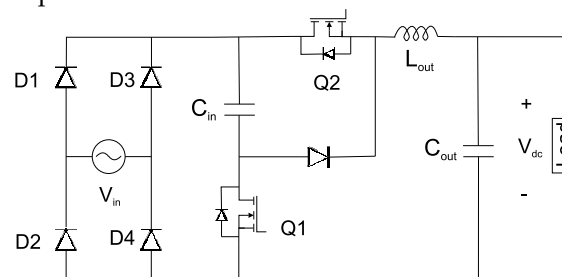


**Figure 12.** Configuration proposed in [85].

The control methodology is defined as ripple confinement control. The configuration is shown in Figure 13. A similar configuration is proposed in [88]. The proposed configuration consists of an additional active switch based on an H-bridge configuration. It requires two capacitors connected at the midpoint and the one end of the inverter legs. The proposed configuration is shown in Figure 14. To mitigate the second-order oscillations in transformerless grid-connected microinverters, a doubly grounded buck-boost (Cuk) topology is proposed in [89]. The incorporated control uses a large swing in the capacitor voltage of the terminal capacitor. It facilitates the usage of film capacitors instead of the less reliable electrolytic capacitors.

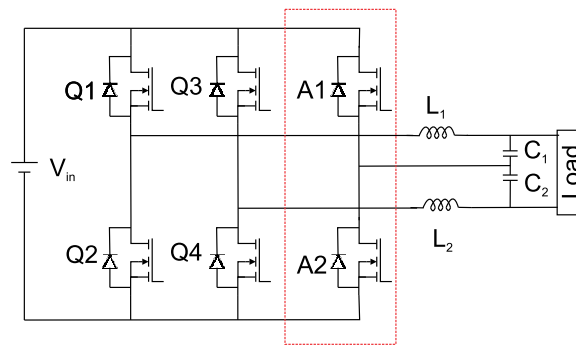


Figure 13. SRC control configuration proposed in [87].

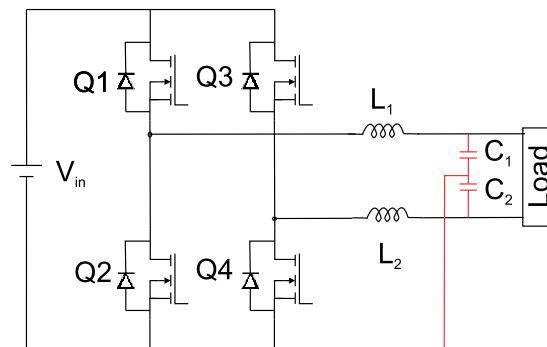


Figure 14. Configuration proposed in [88].

In [90], a combinational power-decoupling method (CPD) is proposed to minimize the bus capacitance required to minimize voltage oscillations and improve the power density for DC–AC power conversions. The configuration can be connected in parallel or series to the conversion stages. The analysis of decoupling for second-order and instantaneous entities is presented. A PFC with sinusoidal current output is presented in [64]. Active power decoupling is used to achieve a low voltage ripple of 8.8% and THD of 4.2%. A power factor of 99% and efficiency of 94.9% is achieved. The topology is shown in Figure 15. A bidirectional single-phase matrix converter with a center-tapped transformer is used for ripple regulation in [91]. The matrix converter uses pulse density modulation so as to achieve zero voltage switching. This will help in improving the efficiency of conversion. The switches of the full bridge inverter can also partially be switches in ZVS. A ripple reduction of 80% was achieved in charging mode, and 76% was achieved in discharging mode. The control has been implemented for battery charging applications. The AC-side THD is regulated to be less than 3%.

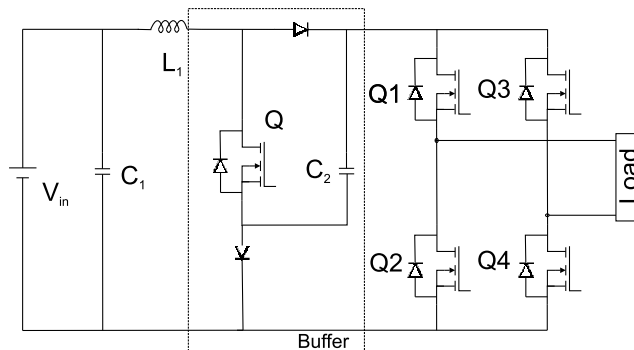


Figure 15. Configuration proposed in [64].

In [92], an SRC mitigation circuitry of a four-switch three-port DC–DC–AC converter is proposed with applications to DC microgrids. The topology consists of three interfaces

of ports that can be connected to the capacitor, DC, or AC ports. In comparison with the H-bridge inverter, the proposed control does not require any extra switches or devices. The control algorithm is also presented. An active control circuit based on a symmetrical half-bridge is proposed in [93]. Small-signal analysis of the proposed configuration is presented. In terms of control, one of the voltage control loops is designed to operate in a stationary frame, while the other loop operates in a synchronous frame. The bandwidth is regulated to achieve acceptable voltage fluctuations during load variations.

The proposed configuration is shown in Figure 16. Similarly, a half-bridge configuration with two capacitors in series is used instead of a single bulky capacitor to mitigate the second-order ripples in [94]. A slight mismatch between the DC component and oscillations in power can be mitigated. The ripple is regulated as per IEEE 1547 standards. The proposed configuration is shown in Figure 17.

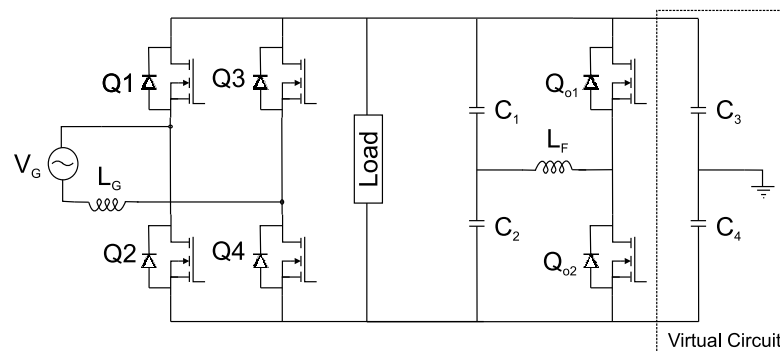


Figure 16. Symmetrical half-bridge configuration proposed in [93].

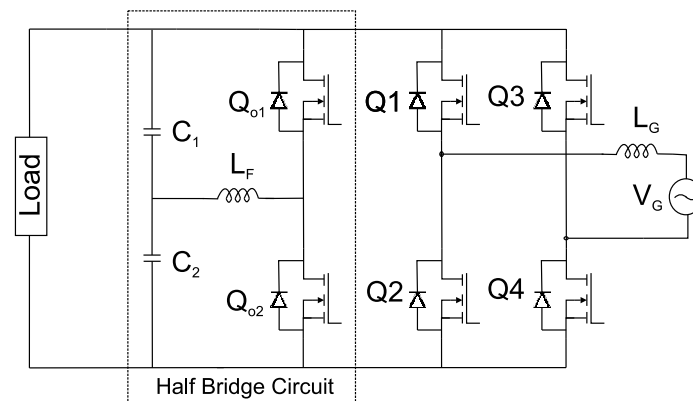


Figure 17. Half-bridge split capacitor proposed in [94].

### 5. Control-Based SRC Mitigation Methodologies

In previous active ripple control methods, extra circuitry is required to absorb the ripple content. The control-based methodologies can increase the impedance virtually. For instance, for the case of a boost converter, the transfer function of output voltage with respect to duty cycle  $T_{vod}$  and inductor current with respect to duty cycle  $T_{iLd} = \frac{\hat{i}_L}{\hat{d}}$  is derived as,

$$T_{vod}(s) = \frac{(1 - D_i)V_o - s(LL_i)}{(LC)s^2 + \frac{sL}{Z} + (1 - D_i)^2}, \tag{3}$$

$$T_{iLd}(s) = \frac{s(CV_{vi}) + 2(1 - D_i)L_i}{(LC)s^2 + \frac{sL}{Z} + (1 - D_i)^2}, \tag{4}$$

where  $D_i$  is duty ratio,  $L$  is inductance,  $C$  is capacitance,  $V_o$  is output voltage,  $Z$  is load inductance, and  $V_{vi}$  is input voltage. These transfer functions are used to derive the control gains. The second-order ripples depend on the impedance of the converter at some specific frequency. In order to reduce ripple current propagation to the source, the impedance must be increased. Virtual impedance is implemented by the inductor current

feedback. If the control consists of an outer voltage controller  $G_v(s)$  and an inner current controller  $G_i(s)$  and the parameter  $K_{pwm}$  is the gain of the PWM, then the transfer function of  $\frac{\hat{v}_o(s)}{\hat{i}_L(s)}|_{\hat{d}=0, \hat{v}_{in}=0, \hat{i}_{Load}=0}$  with  $Z_v(s)$  can be derived to be,

$$\frac{v_o \hat{(s)}}{i_L \hat{(s)}} = \frac{K_{pwm}(sL + \frac{Z_v}{G_N}) + \frac{1}{(1-D)}(V_o G_i - sG_i I_L)}{sL G_v G_i I_L - (1-D)^2 (K_{pwm} + G_v G_i V_o)} \tag{5}$$

From (5), it is observed that the inverted notch  $G_N(s)$  leads to an addition of  $Z_v$  to the output impedance. This value of  $Z_v$  will lead to variations in the impedance magnitude. The loop dynamics with respect to  $Z_v$  is shown in Figure 18. The output impedance variation with respect to the parameter  $Z_v$  is shown in Figure 19. The term  $sL$  is impedance of inductance with respect to frequency and  $1/sC$  is impedance of the output capacitor. It must be noticed that due to the notch filter, the output impedance varies at twice the AC supply frequency, which is 100 Hz for this case.

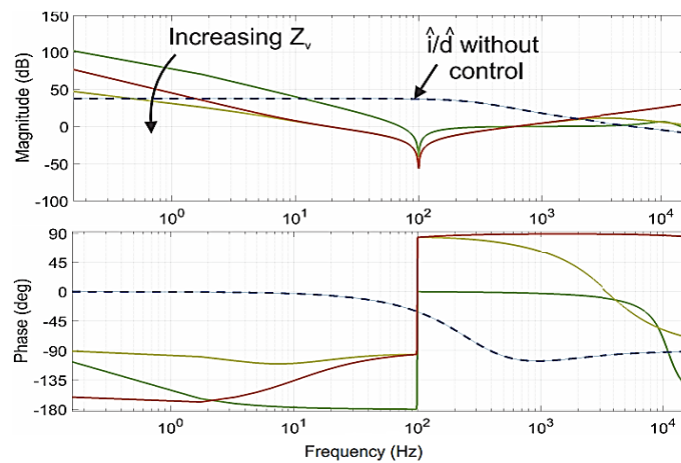


Figure 18. Variation of current control loop with respect to frequency.

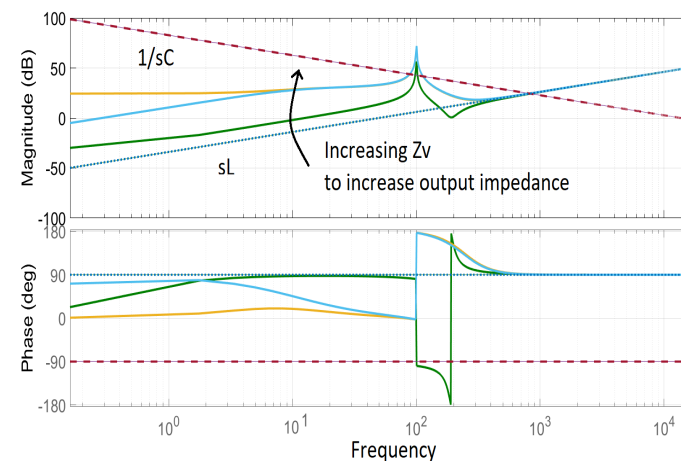


Figure 19. Variation output impedance with  $Z_v$ .

In the literature, different control-based methodologies have been proposed that do not require any external circuit to regulate the ripple content. Hence, such methodologies help reduce the component count. In [95], a load current feedforward methodology has been proposed for SRC control in a two-stage converter. The proposed control regulates the DC bus voltage to oscillate at twice the supply frequency of the AC side. This forces the capacitor at the DC side to supply the ripple power demanded during DC–AC conversions. The control is designed to have minimal impact on the stability and the dynamics of the

system. The control loop implemented is shown in Figure 20, where  $G_v$  is the voltage controller,  $G_d$  is the delay in the sample and hold circuit of the controller, and  $V_{in}$  is the input supply voltage. The load current disturbance is fed to the voltage control loop with the objective of deriving the control law that cancels the SRCs. A bandpass filter is incorporated to filter out the load disturbance at some desired frequency. The ripple current is reduced from 27% to about 1.8% for a 2.5 kW load system. The proposed control law can further be implemented for various other forms of isolated and non-isolated families of converters. Different active filters used to control ripple content are shown in Table 1.

**Table 1.** Summary of active control methodologies.

S.No	Type	Method	Ref.	Connection	Application
(1)	Rectifier	Current source inverter	[63,64]	Parallel	PV panels
(2)	Rectifier	q-Z-source inverter	[65]	Parallel	PV
(3)	Inverter	Push-pull	[56]	Parallel	Fuel cell
(4)	Inverter	Flyback	[96]	Parallel	Fuel cell
(5)	Inverter	Flyback	[97]	Parallel	PV panels
(6)	Inverter	Flyback	[98]	Series	PV, fuel cell
(7)	Inverter	Dual-Boost	[79]	Series	PV panels
(8)	Inverter	Stacked switched capacitor	[67]	Parallel	Capacitor reduction
(9)	Rectification	Differential rectifier	[69]	Parallel	Power factor correction
(10)	Inverter	Switched capacitor	[78]	Series	DC microgrid
(11)	Bidirectional converter	ACRC	[80]	Parallel	AC-DC converters
(12)	Rectifier	Buck converter	[82]	Parallel	Modular multilevel converters
(13)	Rectifier	Buck converter	[81]	Series	Electric vehicle charging
(14)	Rectifier	PFC	[85]	Series	Improve power factor
(15)	Inverter	Cuk derived	[89]	Series	Grid-connected microinverters
(16)	Inverter	Full bridge matrix converter	[91]	Parallel	Battery charge-discharge
(17)	Inverter	Combinational power decoupling	[90]	Parallel	DC-AC conversion
(18)	Inverter	No separate circuit	[92]	Parallel	DC microgrid
(19)	Rectifier	Symmetric half bridge	[93]	Parallel	AC-DC conversions
(20)	Rectifier	Half-bridge split cap.	[94]	Parallel	AC-DC conversions

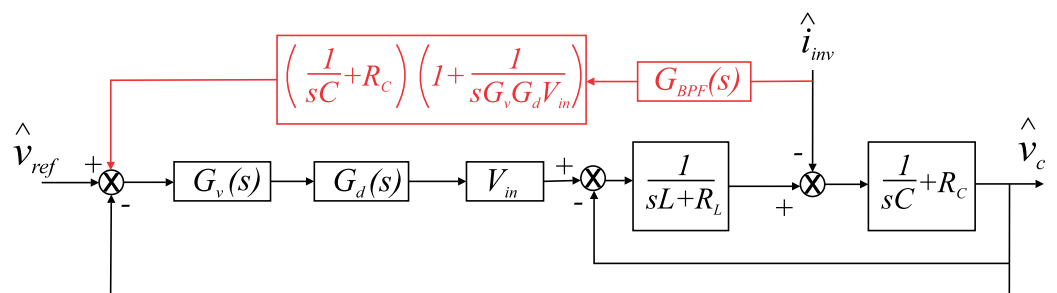


**Figure 20.** Load current feedforward methodology.

In [99], a feedforward control scheme is proposed for ripple control in an LED driver circuit. The driver circuit consists of a power factor correction circuit and a bidirectional converter (BDC). The BDC is responsible for absorption of the ripple components. The control loop implemented is shown in Figure 21. The reference current is phase shifted by negative ninety degrees and multiplied with  $k_1$ , which is a positive constant and is used to regulate the reference value within the sawtooth signal range. The maximum range of the sawtooth signal is  $V_m$ . The proposed control facilitates the use of non-electrolytic capacitors for AC-DC LED drivers.

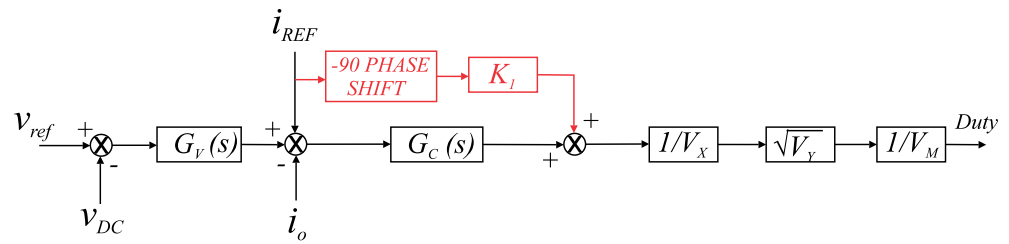


Figure 21. A feedforward control scheme [99].

A resonant controller-based dual-loop control is proposed in [100]. The resonant controller  $G_R$  is used to filter out a component of the signal with some desired frequency. Hence, if the ripple occurs at twice the AC supply frequency, the  $G_R$  is tuned at that frequency. The output of voltage control  $G_v$  is fed to  $G_R$ . This generates the current reference, which is fed to the current controller  $G_i$ . The constant  $T_{PWM}$  is the gain of the PWM generator. The  $T_{dV}$  is the control-to-output-terminal voltage transfer function, and  $T_{di}$  is the control-to-input-current transfer function, as presented in Figure 22. The ripple is reduced from 25% to 5% for a 1500 W load.

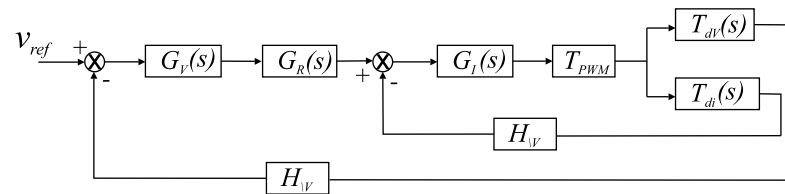


Figure 22. Resonant controller-based dual-loop control [100].

A virtual resistance-based control is proposed in [101] and also presented in Figure 23. In this control methodology, the current from either the inductor or the diode is fed back to the control loop. A constant parameter  $R_v$  regulates the impedance in the inductor branch. However, this control has effect on all the frequencies instead of just  $2f_{ac}$ . This results in degradation of the dynamics of the converter.

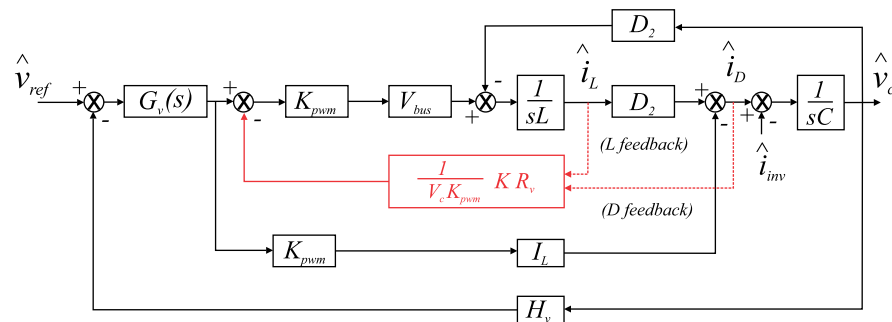


Figure 23. Virtual resistance scheme.

In [52], a bandpass filter-incorporating inductor current feedback scheme (BPFICF) is used to control SRCs. In this scheme, the impedance of the inductor branch is increased virtually at twice the AC supply frequency ( $2f_{ac}$ ). The current can be fed back to the control loop either from the inductor branch or from the capacitor branch, as shown in Figure 24. The magnitude of impedance to be added is  $R_v$ . The transfer function for a bandpass filter is

$$G_{bpf} = \frac{s/Qw_f}{(s/w_f)^2 + s/Q + 1} \tag{6}$$

where  $Q$  is quality factor and  $w_f = 2\pi(2f_{ac})$ . The peak of the BPF can be varied by changing the  $R_v$ , and the frequency at which it occurs can be manipulated by changing  $w_f$ . Further-

more, for diode current feedback,  $K = 1 - \frac{V_{in}}{V_{bus}}$ , and for inductor current feedback,  $K = 1$ . The dynamics are better than the VRS scheme.

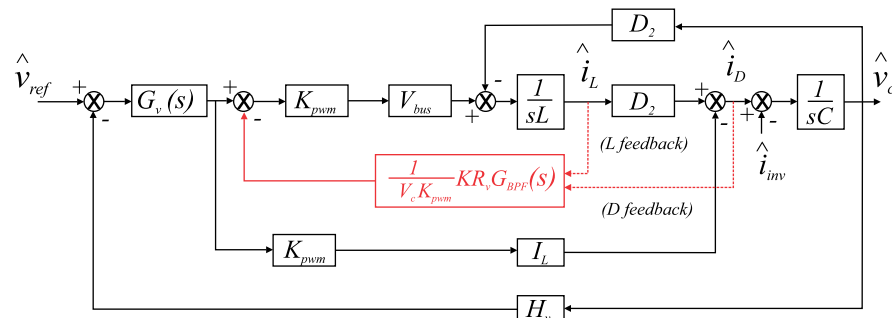


Figure 24. Bandpass filter inductor current feedback scheme.

To further improve the dynamics, a parallel impedance is also added in combination with a series virtual impedance. The scheme is defined as a notch filter-based load current feedforward control scheme (NF-LCFFS) [102]. For this, the current through the capacitor is fed to the control loop through a notch filter. The notch filter is tuned to have a notch at  $2f_{ac}$ .

The transfer function for a notch filter  $G_n$  is

$$G_n = \frac{(s/w_f)^2 + 1}{(s/w_f)^2 + (s/Qw_f) + 1} \tag{7}$$

where  $Q$  is the quality factor and  $w_f = 2\pi(2f_{ac})$ , as for the  $G_{bpf}$  case. The variation of characteristics with  $Q$  is shown in Figure 25. A higher value of  $Q$  leads to a higher notch.

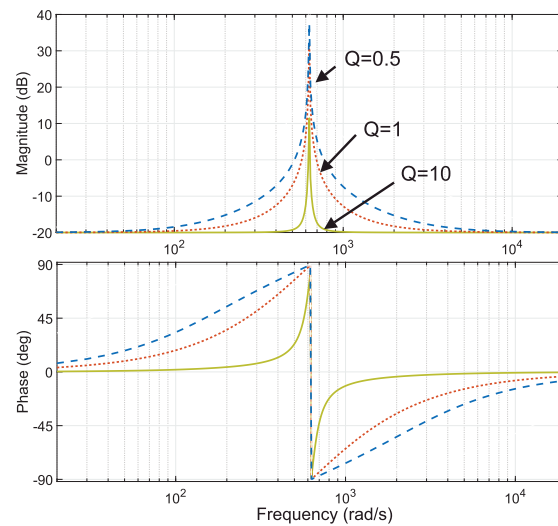


Figure 25. Notch characteristics with different Q-values.

The inner bandpass filter loop remains the same as for the previous case. However, the dynamics obtained is better than with the previous control methodology. The control loops are shown in Figure 26. The bandpass filter can further be removed to obtain a configuration, as shown in Figure 27. The inductor current or diode current is fed by a block that causes the resistive impedance to increase. The value  $R_v$  is the magnitude of the impedance. This control methodology is analogous to the VRS scheme described earlier. This control improved dynamics compared with the VRS scheme; however, it is not as good as the NF-LCFFS scheme. The inverter current can also be fed to the control for two-stage DC-AC conversion applications. The scheme is called the notch filter cascaded voltage

regulator and load current feedforward scheme (NF-VR+LCFFS). The series impedance control is based on a virtual resistance scheme, and the parallel impedance is the notch-fed load current scheme. The proposed control methodology is shown in Figure 28. The term  $D_2 = (1 - D)$ , where  $D$  is the duty ratio of the converter.

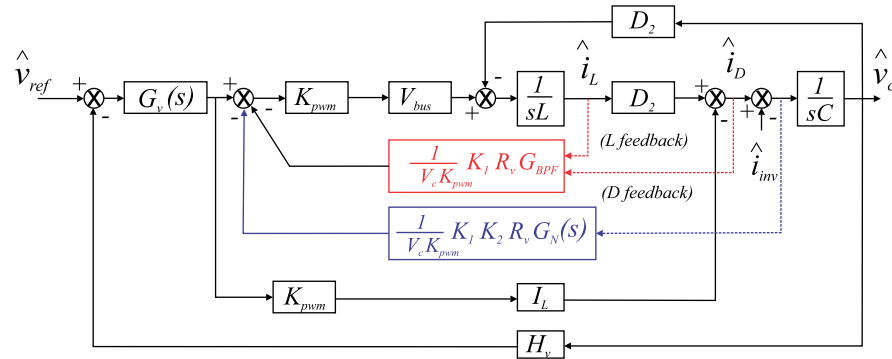


Figure 26. BPFICF with parallel impedance loop.

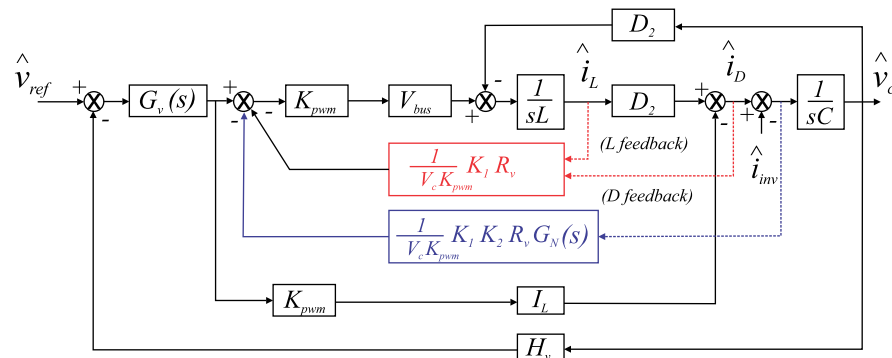


Figure 27. Notch-filter-inserted load current feedforward scheme (NF-LCFFS).

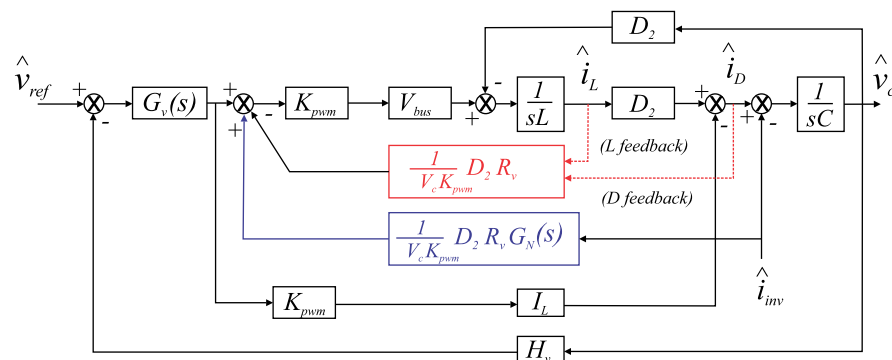


Figure 28. NF-LCFFS with VRS.

### 6. Single-Stage Inverters with Nanogrid Applications

Single-stage inverters are capable of boosting the input DC voltage and performing DC–AC conversion on a single stage. They do not require any separate intermediate boost converter to step up the input DC voltage. The boosting is achieved by a shoot-through mechanism. During shoot-through, the inverter terminals are shorted. No power is transferred from the source to the load during shoot-through. SSIs consist of an impedance network of inductors and capacitors. Z-source inverters (ZSI) were proposed in [103]. A ZSI consists of a pair of a capacitor and an inductor connected in cross-fashion. ZSIs have found applications in PV applications, electric vehicles, and nanogrids. ZSIs have poor input current profiles, and there is voltage stress in the capacitors. As a result, a quasi-Z-source inverter is proposed in [104–106]. qZSIs are used for low- and moderate-power applications.

The different applications of qZSI have been specified in [107–109]. Furthermore, to reduce the voltage and current oscillations due to DC–AC conversions, different solutions have been proposed. An AC equivalent model of a qZSI is derived in [108,110] to analyze the low-frequency ripple in the voltage and source currents. The design of the L, C impedance network for a qZSI is presented in [111,112]. Different configurations of ZSIs/qZSIs have been proposed in the literature with the aim of reducing the stress on the switch and capacitor and improving the input current profile [113–116].

In [114], the authors use a transformer along with the ZSI so as to achieve improved voltage gain compared with traditional ZSIs. Furthermore, an asymmetric TZSI has been proposed in [115] in which the voltage gain is achieved by reducing the turns ratio to unity. The source current is smoother compared to TZSIs. The stress of oscillating voltage across the capacitor is also reduced. The losses in a qZSI increase with the increase in the required voltage gain [117]. However, in fuel-cell and PV applications, a high voltage gain is needed. In order to reduce the size and cost of the SSIs, switched-boost inverters (SBIs) have been proposed in [118–120]. SBIs have a smaller number of components compared with qZSIs; however, an extra active switch is used in the circuitry. SBIs have the disadvantage of discontinuous source currents due to a diode in the input end. The voltage boost of SBIs is less than that of qZSIs. To overcome these drawbacks, various other topologies of quasi-SBIs have been proposed in the literature [121]. The qSBIs are of either the embedded type or the DC link type. An embedded-type qSBI consists of an inductor at the input terminals. An inverse Watkins–Johnson topology-based inverter topology is proposed for DC and AC power applications in [122].

#### *Control of SSIs*

SSIs also suffer from second-order oscillation in the source current and the capacitor voltages similar to the traditional VSIs and CSIs. These SRCs have detrimental effects on the sources and the electrolytic capacitors as discussed earlier. In the literature, different control-based and impedance-shaping methodologies have been used to mitigate SRC propagation to the source. An improved pulse-width strategy is proposed in [123] to achieve maximum voltage boost and to improve the efficiency. In this methodology, the shoot-through duty of one leg is regulated to obtain a desired voltage. This further leads to a reduction in the frequency of switching of the inverter switches by one-third. This reduces the losses due to switching, and hence, the efficiency is improved. A simple boost-modified space vector-based modulation method is proposed in [124] to reduce the number of switch commutations during a switching cycle in a three-phase ZSI. The proposed methodology simplifies the gate signal generation process by the usage of only three reference signals. A hybrid PWM strategy is presented in [125]. The proposed PWM methodology combines the pulse amplitude modulation signal with the pulse width modulation signal. The PWM is designed to operate when the output AC voltage is less than the input DC voltage; otherwise, the PAM operates. In [126], the shoot-through is compared in the negative side and positive side of the repeating sequence. Using this, the signals  $S_a$  and  $S_b$  are generated. These signals are passed through a NAND gate to obtain the desired shoot-through signal, as shown in Figure 29. A robust integral sliding mode control has been proposed for a class of single-stage inverters in [127–129]. The control presented is robust against uncertain operating conditions. To obtain ripple cancellation, the shoot-through can be made to consist of some second-order signal that is related with the second-order component in the source current. This methodology forces the bus capacitor to provide the periodically oscillating power demand. The shoot-through duty on both ends can be made to oscillate with a  $180^\circ$  phase to generate the desired signal, as proposed in [130]. The waveforms for PWM are shown in Figure 30.

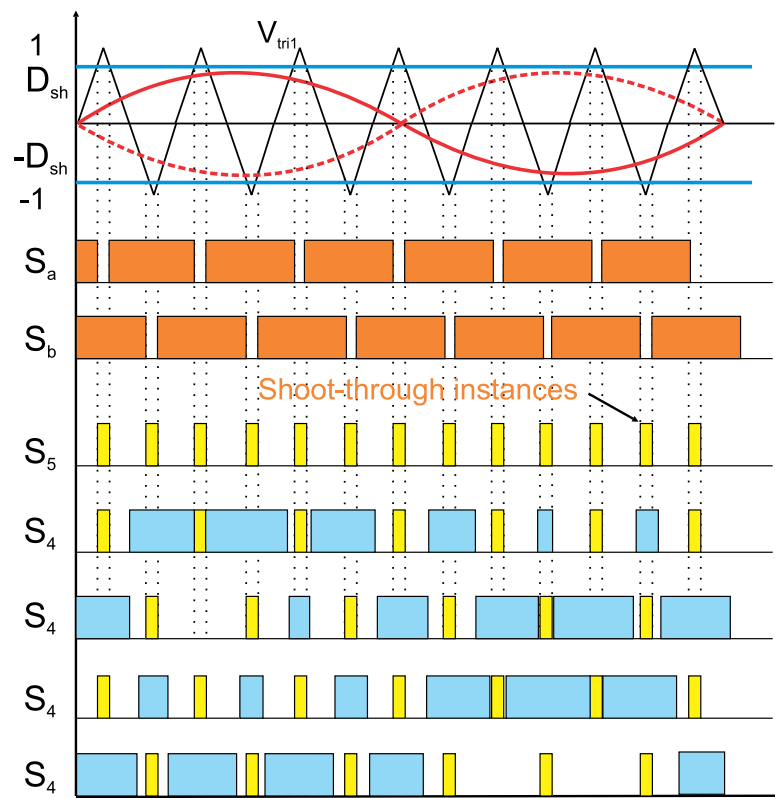


Figure 29. PWM strategy proposed in [126].

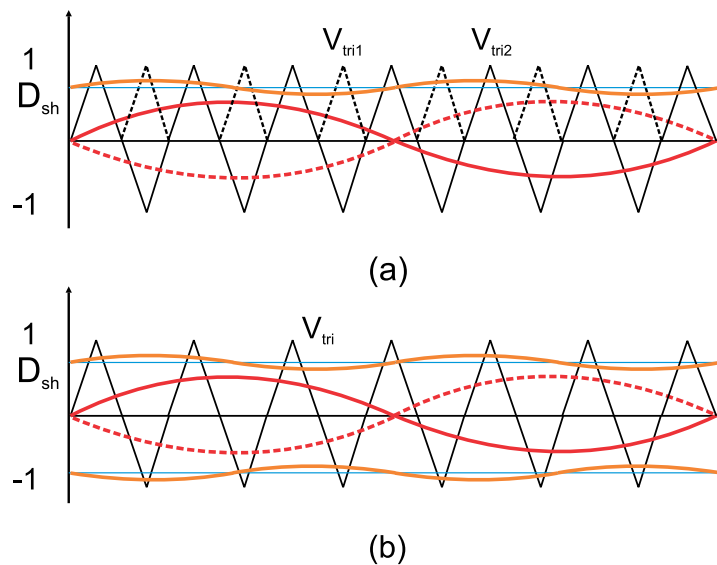


Figure 30. PWM strategy proposed in [130]. (a) Positive shoot through duty (in orange) with two triangular repeating waveforms (in black and dotted). (b) Positive and negative shoot through duty (in orange) with just one repeating signal (in black triangular), desired output sine wave is shown in red.

A constant boost control is proposed in [131] to reduce the voltage and current ripples and improve the voltage gain. A PWM scheme is proposed in [132] to improve the modulation index for SBIs. The proposed PWM methodology leads to fewer second-order ripples in capacitor voltages and inductor currents and a reduction of stress on the switches, with increased efficiency and modulation index value. The conventional PWM generation methodology is shown in Figure 31. The shoot-through duty  $D_{sh}$  is compared with a periodic signal. The shoot-through signal is generated at twice the frequency of the repeating



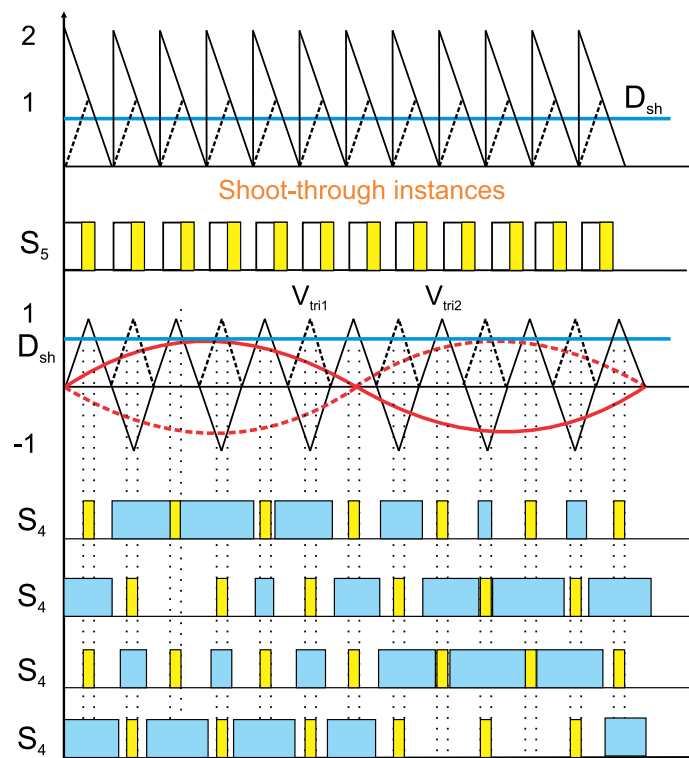


Figure 32. PWM strategy proposed in [132].

## 7. Second-Order Harmonics in Three-Phase System

The second-order harmonics exist on the DC bus of the rectifiers or inverters during the occurrence of the negative sequence voltages. The positive and negative sequences are to be extracted by the unbalanced grid in order to design the ripple control. In [133], the authors extract the unbalanced components using the Clarke transform in a PWM rectifier connected to unbalanced grids. In another method, the positive and negative voltage signals are replaced by the grid voltage and its delayed signal [134]. In [135], the authors have proposed a grid harmonic suppression methodology which does not require the extraction of a negative or positive sequence. The control consists of an improved proportional resonant quasi-controller with minimal dependence on the parameters of the control design. The ripple control design needs to be robust. The control loops usually consist of the active and reactive power references. The direct power control is used, which consists of additions of power compensation to the reference power in order to regulate the unbalanced currents in [136]. The model predictive control-based method has been used in [137] in order to mitigate the second-order ripples in more uncertain unbalanced conditions. The model predictive control with low complexity is proposed in [138] for induction generators under both balanced and unbalanced conditions. With respect to stability, the grid impedance and the grid-connected inverters are coupled, and the overall stability depends on this coupling. In [139], the authors derive the impedance model of the grid-connected converter taking the voltage, current loops and phase-locked loop into consideration. The ripples at the point of coupling voltages are compensated using the proposed methodology. An impedance model of the three-phase four leg grid-connected inverters is derived in [140] considering the positive, negative and zero sequences during unstable grid conditions. Further on, the factors which affect the zero sequence impedances are derived. Analysis of control parameters with respect to electrical distance and stable operating points is presented in [141] in order to ensure stability of the grid-connected inverters. The gains of phase-locked loop vary from small to large, and its effect on the stability is evaluated. Hence, different methodologies have been developed to deal with the unstable grid condition which lead to second-order ripples in the three-phase system. The

second-order ripples also occur in power conversions in microgrids, which is discussed in next section.

## 8. Control of Microgrids

Up to this point, a control for SRC mitigation for SSIs has been presented. In this section, the hierarchical control of DC microgrids is presented. Control can be broadly classified as centralized, decentralized, or distributed control. These methodologies are defined as below:

### 8.1. Centralized Control

In centralized control, the voltage and current measurements are sent to a central node. The data from each node are processed and the corresponding references are generated for individual nodes. The voltage and current data are used by the centralized control to evaluate which node is more loaded and which is less so. Accordingly, it takes the action of increasing or reducing the voltage references. Furthermore, optimization algorithms can also be implemented to maximize the value of the microgrid and to achieve minimal cost of operation when operating with multiple sources. Load-side management schemes can also be implemented [142,143]. Centralized control can easily manage the energy flow, i.e., in the presence of surplus energy, it can activate energy storage, while in energy deficit, it can activate the backup supplies such as diesel generators, etc. [144]. Centralized control has the advantage of easier control and implementation [145]. However, if the central control does not function in the desired way, the microgrid may become unstable or failure may occur. Hence, it is applicable for a small-scale microgrid system [146]. A centralized control scheme is shown in Figure 33a. Another disadvantage is higher dependence on communication exchange, as a greater number of channels are required to facilitate transfer of communication values.

### 8.2. Decentralized Control

A decentralized control scheme does not require communication among the interfaced nodes of the DC microgrid. The desired global operating conditions are obtained from only the local information of the node. A simple example of decentralized control is droop control. In this, the voltage reference of a node is reduced if it is more loaded. This helps in load distribution between the nodes. An example of decentralized control is shown in Figure 33b.

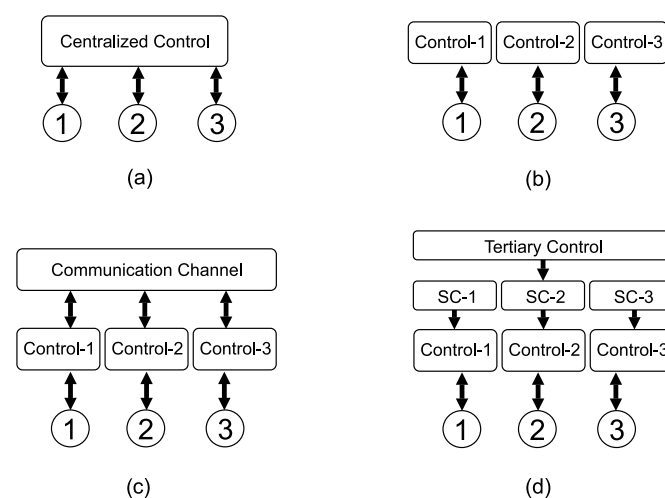


**Figure 33.** Concept of centralized and decentralized control: (a) Centralized control. (b) Decentralized individual control. (c) Distributed control with communication channel. (d) Multiple control levels as primary, secondary control (sc), and tertiary controls.

### 8.3. Distributed Control

To improve the reliability and performance of a microgrid, different control schemes are used, thereby integrating the management part with the decentralized control. Different communication technologies such as WiFi, Zigbee, etc. [147] are used with distributed algorithms such as consensus-based control, gossip algorithm, etc. [148–152]. Decentralized control with communication is shown in Figure 33c. However, maintaining the coordination between the controllers at different nodes still remains a challenge. An example of distributed control is shown in Figure 33d. An example of distributed control is the hierarchical control of microgrids. Hierarchical control consists of a primary control that operates at a node, a secondary control that receives the communication data and estimates the references for the primary control, and finally, a tertiary control that controls a cluster of microgrids. The load distribution in a large-scale microgrid is completed by the tertiary control. It generates the reference for the secondary control. The configuration of control is shown in Figure 34. The figure shows an overview of the tasks performed by an individual controller.

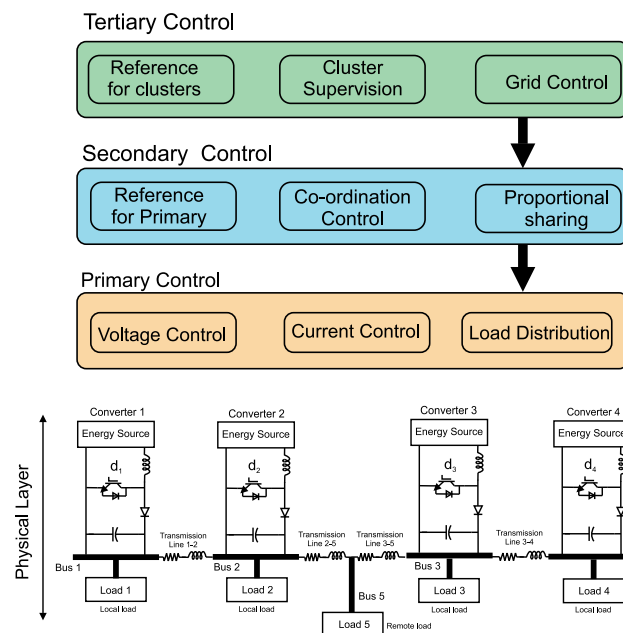


Figure 34. Control hierarchy for microgrids.

#### 8.3.1. Primary Control

The primary control layer operates to regulate the local voltage and current as desired. It receives the reference from the upper layers of the hierarchical control. In the literature, different forms of primary control have been proposed. Droop control manages the voltage reference at a node depending on the loading condition of that node. Different control methodologies have been proposed in the literature. Traditional droop control is used to achieve load sharing without any need for data transfer between the nodes [6,153,154]. Droop control is easy to implement, as only local values are needed. In [155], a master-slave control is proposed to achieve load sharing. One of the nodes is considered to be the master, and the other nodes follow the parameters of the master node. To improve fault tolerance and detection, a circular chain control configuration is proposed in [156]. To improve the performance of the microgrid under heavy loading conditions, various nonlinear droop control methodologies have also been proposed. An efficiency-based virtual resistance is designed in [157] for load sharing. A real-time-based multi-agent control for an electric ship is proposed in [158,159]. A similar nonlinear droop is proposed in [159]. A DC bus signaling-based control for the selection of mode of operation has been presented in [160,161]. The modes of operation are grid-connected, islanding with battery discharging, and islanding and grid-connected rectification.

### 8.3.2. Secondary Control

Primary droop control results in poor voltage regulation when the load is varied from no load to full load. The secondary control is responsible for generating an adequate voltage reference shift to improve the voltage regulation. Secondary control is used to achieve proportional load sharing, synchronization of different nodes, and good voltage regulation [160]. In [162], low-bandwidth data exchange is used to exchange the voltage and current data between neighboring nodes to achieve load sharing in proportion to the rated capacity. These values are compared with local values, and adequate voltage and current reference shifts are generated to achieve proportional load sharing. A distributed team-oriented load sharing-based secondary control is proposed to achieve good voltage regulation and minimization of circulating currents between the nodes in [163]. Current sharing among nodes is further improved in [164]. The proposed control uses slope-adjusting approaches to adjust the droop coefficients depending on the command signal from the secondary control. Secondary control for AC microgrids is presented in [165]. It regulates the frequency deviations due to load variations. Distributed control for reactive power sharing and maintaining voltage stability is proposed in [166]. A distributed averaging-based secondary control for islanded microgrids is formulated in [167]. A linear matrix inequality-based control is proposed in [168] to facilitate smooth plug-and-play control in microgrids. The proposed control operated in all-to-all communication mode or in minimal communication modes with the condition that the network should have at least a spanning tree, as shown in Figure 35. The node in red shows that it may be disconnected from the microgrid so as to operate in islanded mode. Hence, plug-and-play features must also be addressed. A robust integral sliding mode control mode-based secondary control is proposed in [6] to maintain desired operations during communication uncertainties.

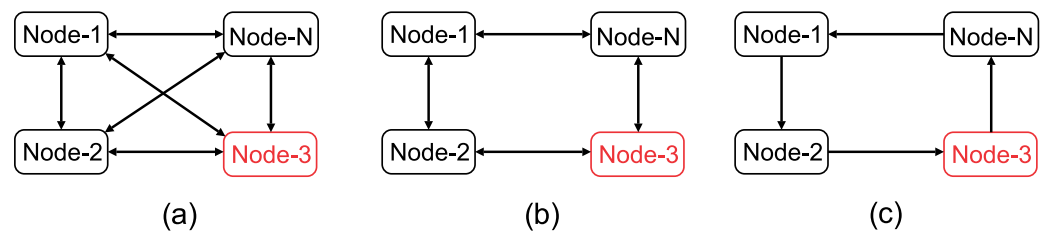


Figure 35. Communication: (a) all-to-all, (b) neighboring, (c) sparse.

### 8.3.3. Tertiary Control

The function of tertiary control is to manage power flow within the cluster of microgrids and to minimize the operating cost. Tertiary control is necessary to improve the reliability of the microgrid. It also ensures proper coordination between the energy storage and generation units [169,170] by using the Newton–Raphson method for computation. Similar power calculations can be performed for DC microgrid applications with the availability of terminal voltage measurements, as in [171,172]. Furthermore, economic load dispatch is focused on in the research works of [173,174]. Various parallel computation algorithms have also been proposed to optimize the performance of the microgrid system [175,176]. Tertiary control is shown in Figure 36. The connection with dotted lines shows that the node can be removed or added to the network.

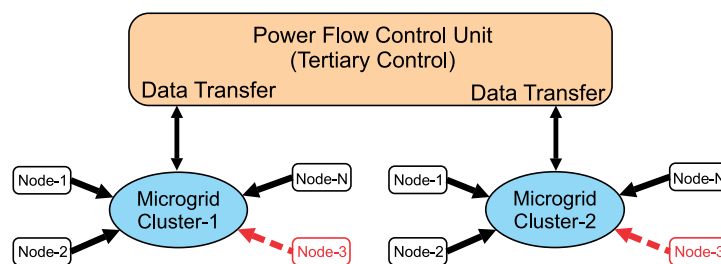


Figure 36. Tertiary control.

#### 8.3.4. Ripple Management in Microgrids

A DC–AC conversion leads to second-order oscillations in the DC bus voltage and source currents. These oscillations can also occur when DC microgrids are integrated with AC microgrids or grid-forming inverters (GFIs) [177]. The DC bus voltage is controlled to be within the desired voltage regulation limits. As a result of this, SRCs are visible in the source currents. In a microgrid environment, in the presence of primary and secondary control, the SRC is shared as per the proportional load sharing among the interfaced nodes. However, a source with a higher power rating may not have a high SRC-bearing capability. In addition, a ripple filter can be installed at a node, and all the ripples must be propagated to this node. The concept is presented in Figure 37. The figure shows four nodes with  $R_{Line1}$ – $R_{Line4}$ , which affect the load sharing among the sources. Each node has its local load  $R_{Load1}$ – $R_{Load4}$ . The inverter-fed AC load is connected to the DC bus which leads to ripple current being drawn from the sources. These second-order ripple currents can be managed by managing the impedance at each node virtually. Each node consists of its own virtual impedance control which operates at the ripple frequency. The node with higher virtual impedance has to supply less ripple current compared to the node with lesser impedance. There are three types of loads, constant resistive loads, constant power loads (CPLs), and also inverter-fed AC loads. CPLs tend to make microgrids unstable [178]. The ripples in source current and bus voltage occur at twice the AC supply frequency. The figure shows the physical layer and the cyber layer. The data are exchanged among the nodes through the cyber layer. The primary controller is designed to regulate the output impedance of the converters to manage the ripple content in the voltage or current as per the requirement. In the literature, some ripple-sharing methodologies have been proposed. In [179], the authors propose an oscillatory current, and DC load is shared as per the rating of the converter. The current control consists of a DC and oscillatory current control block, and a multi-loop voltage control is employed to regulate the DC bus voltage. In [180], an impedance controller is integrated with a dual-loop proportional–integral controller. This impedance controller varies the output impedance based on the ripple reference provided. The ripple reference is decided based on the ripple absorbing capacity of the source node. The proposed control has been verified to operate with PI-based secondary control. Another SRC suppression methodology is proposed in [181]. The proposed control uses a notch filter and resonance regulators in the control loop. The bandwidth of the voltage control loop is below twice the AC supply frequency. This will lead to a degradation of dynamics. Furthermore, in [182], a power-oscillations damping control is proposed to regulate SRCs. The proposed control uses a droop that changes dynamically in order to actively damp the oscillations due to DC–AC conversions. Pole placement and small-signal analysis are used to design the virtual impedance control. The control has been verified for a hybrid system consisting of a fuel cell, a supercapacitor, and a photovoltaic system. In the literature, different robust control methodologies have been proposed to regulate SRCs in nanogrids and DC microgrids. The nanogrids consist of single-stage inverters. In [183], an adaptive sliding mode control primary control has been proposed to regulate the ripple current among the interfaced converters. The adaptive controller is interfaced with consensus-based secondary control to achieve proportional load sharing among the source nodes. The sliding manifold changes adaptively with respect to the DC bus voltage and node current conditions. The proposed control can be operated even in uncertain operation conditions.

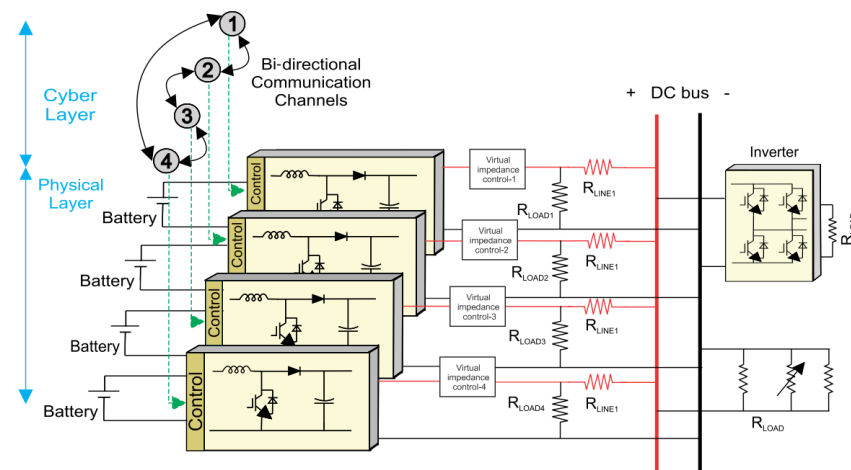


Figure 37. Virtual impedance control at nodes of microgrid.

## 9. Concluding Discussion

Second-order ripples are one of the most common issues during DC–AC or AC–DC conversions. Hence, different methodologies have been proposed in literature. Methods which consist of the implementation of active or passive filters require additional components which lead to an increased cost of the overall system. The benefit of using an active ripple control method is that it leads to ripple reduction with much fewer passive components, thereby increasing reliability and reducing cost. On the other hand, there are virtual impedance-based ripple control methods. These methods consist of designing the control loops which result in ripple reduction. The gain margin of the control loops is varied at the ripple frequency, which emulates a varying impedance at the terminals of the converter. The virtual impedance control method does not require additional components, but the control loops must be designed carefully so as not to affect the dynamic performance of the converter. The virtual impedance control loop usually consists of a low pass, bandpass or a notch filter which affects the dynamic performance if not designed properly. In order to achieve this, a separate ripple control loop can be incorporated that manages the impedance based on the ripple content. The ripple magnitude can be extracted from the voltage or current signal using a second-order general integrator, and this can then be compared with the desired ripple content. Furthermore, in terms of microgrid, the virtual impedance control can be implemented in the primary control. The primary control can be equipped with virtual impedance control which results in higher or lower impedances based on the passive component availability at the node, such that the node with an active ripple filter or higher capacitance can share more second-order ripples than the others with lower ratings or lower passive components. Implementing second-order ripple sharing with only passive components will be a challenge, but the implementation of virtual impedance control will make the ripple sharing more flexible and simple. Hence, in most of the cases, the virtual impedance control has an advantage over traditional active or passive control methods. The only disadvantage is the limitation of operation, such as modulation indexes or ripples in DC bus voltages, which needs to be taken care of.

## 10. Conclusions and Open Challenges

This manuscript presents different methodologies adopted in the literature to mitigate the second-order ripples with respect to microgrids, single-stage inverters, and DC–AC topologies. Initially, active and passive control methodologies for ripple mitigation are presented. Increasing the passive components leads to an increase in the weight, dimensions, and cost of the system. An increase of capacitance will lead to a decrease in the reliability of the system as the low-cost electrolytic capacitors have a smaller lifespan compared with the non-electrolytic capacitors. To reduce the capacitance required, various active filters are

used. The active filters consist of a series or parallel arrangement of filters. They consist of a capacitor or inductor as the ripple energy storage element. The filters absorb the second-order ripple energy in one cycle and release the energy in the other cycle. However, this leads to an increased component count, which in turn leads to an increased cost of the system. To maintain the components count, different modulation-based techniques have been proposed. The limitation of such a methodology is to mitigate the ripple content by signal injection with the modulation while keeping the total harmonic distortion within acceptable limits. There are limitations to the upper limit of the magnitude of the injected signal such that it does not affect the normal operation of the DC–AC stage. This issue becomes more prevalent in single-stage inverters that incorporate the shoot-through of switches in order to achieve a higher-output AC voltage. In the literature, different virtual impedance methodologies have been proposed to mitigate ripples in DC–AC and SSI converters. The virtual impedance designed is of constant magnitude, while the SRC content keeps on varying as per the AC loading condition.

The control consists of linear controllers whose performance may degrade in cases of modeling or operating condition uncertainties. Increased impedance with less AC load leads to a degradation of dynamics. Hence, the impedance shaping must be dynamic in nature. DC microgrids also suffer from SRCs when the AC load is connected to the DC bus. In the absence of any control, the SRCs become divided such that the node with lower impedance obtains a greater share of the SRCs. The source installed at a node may have a higher rating, but the impact of an SRC on it can be severe. This leads to a reduction in the lifespan of the sources. Similarly, the SRC filter circuit may not be installed at all the nodes of the microgrid. Hence, there is a need to divert all the SRCs from a load to a specific node that has a ripple filter circuit installed. In a distributed control architecture such as a DC microgrid, feeding the load currents, which are spread throughout the network, is not feasible. It will make the system more complex, as the data exchange will increase and a larger communication bandwidth will have to be incorporated. The possible solution must consist of minimal dependence on the neighboring data so as to implement the ripple control with the existing communication facility. Different nonlinear controllers can be implemented such that they can regulate impedance with local node dynamics. Furthermore, the designed control must not affect the dynamics of the system under all loading conditions and must not be affected due to uncertainties present in the system. The designed solution must reduce ripple content irrespective of other unknown matched or unmatched uncertainties. The controllers based on integral sliding-mode control are capable of operating in uncertain operating conditions. Such controllers can be implemented. The effect of the control methodology on the lifespan of the components must also be evaluated. Strategies can be implemented that will be incorporated to regulate the source temperature with respect to the ripple current magnitude.

To summarize, the control of second-order ripples is necessary but must be regulated without affecting the dynamic performance of the converter or the network of converters. It must be able to operate in an adaptive fashion and should lead to an improved lifespan of the components as a whole.

**Author Contributions:** Methodology, S.C. and G.V.H.; Formal analysis, S.C. and S.A.K.; Writing—original draft, S.C.; Writing—review & editing, S.C. and D.F.; Visualization, Y.F.; Supervision, M.W.; Project administration, M.W. and W.S. All authors have read and agreed to the published version of the manuscript.

**Funding:** This research received no external funding.

**Conflicts of Interest:** The authors declare no conflict of interest.

## References

1. Wang, J.; Wu, H.; Yang, T.; Zhang, L.; Xing, Y. Bidirectional three-phase DC–AC converter with embedded DC–DC converter and carrier-based PWM strategy for wide voltage range applications. *IEEE Trans. Ind. Electron.* **2018**, *66*, 4144–4155. [[CrossRef](#)]
2. Wang, J.; Sun, K.; Zhou, D.; Li, Y. Virtual SVPWM-Based Flexible Power Control for Dual-DC-Port DC–AC Converters in PV–Battery Hybrid Systems. *IEEE Trans. Power Electron.* **2021**, *36*, 11431–11443. [[CrossRef](#)]
3. Milbradt, D.M.C.; Hollweg, G.V.; de Oliveira Evald, P.J.D.; da Silveira, W.B.; Gründling, H.A. A robust adaptive One Sample Ahead Preview controller for grid-injected currents of a grid-tied power converter with an LCL filter. *Int. J. Electr. Power Energy Syst.* **2022**, *142*, 108286. [[CrossRef](#)]
4. Hollweg, G.V.; de Oliveira Evald, P.D.; Tambara, R.V.; Grundling, H.A. Adaptive super-twisting sliding mode for dc-ac converters in very weak grids. *Int. J. Electron.* **2022**. [[CrossRef](#)]
5. Evald, P.J.; Hollweg, G.V.; Mattos, E.; Borin, L.; Tambara, R.; Montagner, V. A Least-Square-based RMRAC for Grid-tied Voltage Source Inverters with LCL Filter. In Proceedings of the 2022 14th Seminar on Power Electronics and Control (SEPOC), Santa Maria, Brazil, 2–15 November 2022; IEEE: Piscataway, NJ, USA, 2022; pp. 1–6.
6. Chaturvedi, S.; Fulwani, D. Adaptive Voltage Tuning Based Load Sharing in DC Microgrid. *IEEE Trans. Ind. Appl.* **2021**, *57*, 977–986. [[CrossRef](#)]
7. Nami, A.; Rodriguez-Amenedo, J.L.; Arnaltes, S.; Cardiel-Alvarez, M.A.; Baraciarte, R.A. Control of the Parallel Operation of DR-HVDC and VSC-HVDC for Offshore Wind Power Transmission. *IEEE Trans. Power Deliv.* **2022**, *37*, 1682–1691. [[CrossRef](#)]
8. Rao, H.; Zhou, Y.; Xu, S.; Cai, X.; Cao, W.; Xu, Y.; Ren, C. Key technologies of ultra-high voltage hybrid LCC-VSC MTDC systems. *CSEE J. Power Energy Syst.* **2019**, *5*, 365–373. [[CrossRef](#)]
9. Nejabatkhah, F.; Li, Y.W. Overview of Power Management Strategies of Hybrid AC/DC Microgrid. *IEEE Trans. Power Electron.* **2015**, *30*, 7072–7089. [[CrossRef](#)]
10. Wei, B.; Han, X.; Wang, P.; Yu, H.; Li, W.; Guo, L. Temporally Coordinated Energy Management for AC/DC Hybrid Microgrid Considering Dynamic Conversion Efficiency of Bidirectional AC/DC Converter. *IEEE Access* **2020**, *8*, 70878–70889. [[CrossRef](#)]
11. Li, X.; Guo, L.; Li, Y.; Guo, Z.; Hong, C.; Zhang, Y.; Wang, C. A Unified Control for the DC–AC Interlinking Converters in Hybrid AC/DC Microgrids. *IEEE Trans. Smart Grid* **2018**, *9*, 6540–6553. [[CrossRef](#)]
12. Xia, Y.; Wei, W.; Yu, M.; Wang, X.; Peng, Y. Power Management for a Hybrid AC/DC Microgrid With Multiple Subgrids. *IEEE Trans. Power Electron.* **2018**, *33*, 3520–3533. [[CrossRef](#)]
13. Liu, Q.; Caldognetto, T.; Buso, S. Review and comparison of grid-tied inverter controllers in microgrids. *IEEE Trans. Power Electron.* **2019**, *35*, 7624–7639. [[CrossRef](#)]
14. Zhang, H.; Xiang, W.; Lin, W.; Wen, J. Grid forming converters in renewable energy sources dominated power grid: Control strategy, stability, application, and challenges. *J. Mod. Power Syst. Clean Energy* **2021**, *9*, 1239–1256. [[CrossRef](#)]
15. Hollweg, G.V.; de Oliveira Evald, P.J.D.; Tambara, R.V.; Gründling, H.A. A Robust Adaptive Super-Twisting Sliding Mode Controller applied on grid-tied power converter with an LCL filter. *Control Eng. Pract.* **2022**, *122*, 105104. [[CrossRef](#)]
16. Ziouani, I.; Boukhetala, D.; Darcherif, A.M.; Amghar, B.; El Abbassi, I. Hierarchical control for flexible microgrid based on three-phase voltage source inverters operated in parallel. *Int. J. Electr. Power Energy Syst.* **2018**, *95*, 188–201. [[CrossRef](#)]
17. Dias de Oliveira Evald, P.J.; Vieira Hollweg, G.; Varella Tambara, R.; Gründling, H.A. A new discrete-time PI-RMRAC for grid-side currents control of grid-tied three-phase power converter. *Int. Trans. Electr. Energy Syst.* **2021**, *31*, e12982. [[CrossRef](#)]
18. Hollweg, G.V.; Paulo, J.d.O.; Mattos, E.; Borin, L.; Tambara, R.; Montagner, V. Optimized Parameters Initialization of a RMRAC Controller Applied to Grid-Connected Converters. In Proceedings of the 2022 14th Seminar on Power Electronics and Control (SEPOC), Santa Maria, Brazil, 2–15 November 2022; IEEE: Piscataway, NJ, USA, 2022; pp. 1–6.
19. Tang, Y.; Blaabjerg, F.; Loh, P.C.; Jin, C.; Wang, P. Decoupling of Fluctuating Power in Single-Phase Systems Through a Symmetrical Half-Bridge Circuit. *IEEE Trans. Power Electron.* **2015**, *30*, 1855–1865. [[CrossRef](#)]
20. Singh, A.; Mirafzal, B. An efficient grid-connected three-phase single-stage boost current source inverter. *IEEE Power Energy Technol. Syst. J.* **2019**, *6*, 142–151. [[CrossRef](#)]
21. Wang, Z.; Xu, Y.; Liu, P.; Zhang, Y.; He, J. Zero-voltage-switching current source inverter fed PMSM drives with reduced EMI. *IEEE Trans. Power Electron.* **2020**, *36*, 761–771. [[CrossRef](#)]
22. Gautam, A.R.; Gourav, K.; Guerrero, J.M.; Fulwani, D.M. Ripple Mitigation With Improved Line-Load Transients Response in a Two-Stage DC–DC–AC Converter: Adaptive SMC Approach. *IEEE Trans. Ind. Electron.* **2018**, *65*, 3125–3135. [[CrossRef](#)]
23. Zhang, L.; Ruan, X.; Ren, X. Second-Harmonic Current Reduction and Dynamic Performance Improvement in the Two-Stage Inverters: An Output Impedance Perspective. *IEEE Trans. Ind. Electron.* **2015**, *62*, 394–404. [[CrossRef](#)]
24. Nguyen, M.; Lim, Y.; Cho, G. Switched-Inductor Quasi-Z-Source Inverter. *IEEE Trans. Power Electron.* **2011**, *26*, 3183–3191. [[CrossRef](#)]
25. Peng, F.Z.; Yuan, X.; Fang, X.; Qian, Z. Z-source inverter for adjustable speed drives. *IEEE Power Electron. Lett.* **2003**, *1*, 33–35. [[CrossRef](#)]
26. Fontes, G.; Turpin, C.; Astier, S.; Meynard, T.A. Interactions Between Fuel Cells and Power Converters: Influence of Current Harmonics on a Fuel Cell Stack. *IEEE Trans. Power Electron.* **2007**, *22*, 670–678. [[CrossRef](#)]
27. Palma, L.; Todorovic, M.H.; Enjeti, P. Design considerations for a fuel cell powered DC–DC converter for portable applications. In Proceedings of the Twenty-First Annual IEEE Applied Power Electronics Conference and Exposition, Dallas, TX, USA, 19–23 March 2006.

28. Peng, F.Z.; Li, H.; Su, G.-J.; Lawler, J.S. A new ZVS bidirectional DC-DC converter for fuel cell and battery application. *IEEE Trans. Power Electron.* **2004**, *19*, 54–65. [[CrossRef](#)]
29. Boscaino, V.; Miceli, R.; Buccella, C.; Cecati, C.; Latafat, H.; Razi, K. Fuel Cell power system with LLC resonant DC/DC converter. In Proceedings of the 2014 IEEE International Electric Vehicle Conference (IEVC), Florence, Italy, 17–19 December 2014; pp. 1–6.
30. Xu, H.; Kong, L.; Wen, X. Fuel cell power system and high power DC-DC converter. *IEEE Trans. Power Electron.* **2004**, *19*, 1250–1255. [[CrossRef](#)]
31. Choi, W.; Enjeti, P.N.; Howze, J.W. Development of an equivalent circuit model of a fuel cell to evaluate the effects of inverter ripple current. In Proceedings of the Nineteenth Annual IEEE Applied Power Electronics Conference and Exposition, Anaheim, CA, USA, 22–26 February 2004; Volume 1, pp. 355–361.
32. Li, X.; Zhang, W.; Li, H.; Xie, R.; Chen, M.; Shen, G.; Xu, D. Power Management Unit With Its Control for a Three-Phase Fuel Cell Power System Without Large Electrolytic Capacitors. *IEEE Trans. Power Electron.* **2011**, *26*, 3766–3777. [[CrossRef](#)]
33. Jin, K.; Ruan, X.; Yang, M.; Xu, M. A Hybrid Fuel Cell Power System. *IEEE Trans. Ind. Electron.* **2009**, *56*, 1212–1222. [[CrossRef](#)]
34. Kim, T.; Jeong, J.-B.; Lee, B.-H.; Shin, D.-H.; Song, H.-S.; Kim, B.-H.; Kim, H.-J. Analytical study on low-frequency ripple effect of battery charging. In Proceedings of the 2012 IEEE Vehicle Power and Propulsion Conference, Seoul, Korea, 9–12 October 2012; pp. 809–811.
35. *IEEE Std 1184-2006*; IEEE Guide for Batteries for Uninterruptible Power Supply Systems. IEEE: Piscataway, NJ, USA, 2006; pp. 1–63. [[CrossRef](#)]
36. *IEEE Std 519-2014 (Revision of IEEE Std 519-1992)*; IEEE Recommended Practice and Requirements for Harmonic Control in Electric Power Systems. IEEE: Piscataway, NJ, USA, 2014; pp. 1–29.
37. *IEEE Std 1188-2005 (Revision of IEEE Std 1188-1996)*; IEEE Recommended Practice for Maintenance, Testing, and Replacement of Valve-Regulated Lead-Acid (VRLA) Batteries for Stationary Applications. IEEE: Piscataway, NJ, USA, 2006; pp. 1–44. [[CrossRef](#)]
38. *IEEE P485/D2*; IEEE Draft Recommended Practice for Sizing Lead-Acid Batteries for Stationary Applications. IEEE: Piscataway, NJ, USA, 2016; pp. 1–67.
39. *P1115/D4*; IEEE Draft Recommended Practice for Sizing Nickel-Cadmium Batteries for Stationary Applications. IEEE: Piscataway, NJ, USA, 2014; pp. 1–37.
40. Kan, S.; Ruan, X.; Dang, H.; Zhang, L.; Huang, X. Second Harmonic Current Reduction in Front-End DC DC Converter for Two-Stage Single-Phase Photovoltaic Grid-Connected Inverter. *IEEE Trans. Power Electron.* **2019**, *34*, 6399–6410. [[CrossRef](#)]
41. Lin, S.L.; Wu, G.B.; Liu, W.; Moo, C.S. Ripple current effect on output power of solar-cell panel. In Proceedings of the 2012 International Conference on Renewable Energy Research and Applications (ICRERA), Nagasaki, Japan, 11–14 November 2012; pp. 1–5.
42. Brunton, S.L.; Rowley, C.W.; Kulkarni, S.R.; Clarkson, C. Maximum Power Point Tracking for Photovoltaic Optimization Using Ripple-Based Extremum Seeking Control. *IEEE Trans. Power Electron.* **2010**, *25*, 2531–2540. [[CrossRef](#)]
43. Casadei, D.; Grandi, G.; Rossi, C. Single-phase single-stage photovoltaic generation system based on a ripple correlation control maximum power point tracking. *IEEE Trans. Energy Convers.* **2006**, *21*, 562–568. [[CrossRef](#)]
44. Ishaque, K.; Salam, Z.; Amjad, M.; Mekhilef, S. An Improved Particle Swarm Optimization (PSO)-Based MPPT for PV With Reduced Steady-State Oscillation. *IEEE Trans. Power Electron.* **2012**, *27*, 3627–3638. [[CrossRef](#)]
45. Sullivan, C.R.; Awerbuch, J.J.; Latham, A.M. Decrease in Photovoltaic Power Output from Ripple: Simple General Calculation and the Effect of Partial Shading. *IEEE Trans. Power Electron.* **2013**, *28*, 740–747. [[CrossRef](#)]
46. Liu, Y.; Ge, B.; Abu-Rub, H.; Sun, D. Comprehensive Modeling of Single-Phase Quasi-Z-Source Photovoltaic Inverter to Investigate Low-Frequency Voltage and Current Ripple. In Proceedings of the 2014 IEEE Energy Conversion Congress and Exposition (ECCE), Pittsburgh, PA, USA, 14–18 September 2014; pp. 4226–4231.
47. Benavides, N.D.; Chapman, P.L. Modeling the effect of voltage ripple on the power output of photovoltaic modules. *IEEE Trans. Ind. Electron.* **2008**, *55*, 2638–2643. [[CrossRef](#)]
48. Bati, A.; Luk, P.C.K. Analysis of drive-train resonance and torque ripple smoothing of a 50kW vertical axis wind turbine. In Proceedings of the 2015 IEEE International Conference on Industrial Technology (ICIT), Seville, Spain, 17–19 March 2015; pp. 1263–1268.
49. Xia, Y.Y.; Fletcher, J.E.; Finney, S.J.; Ahmed, K.H.; Williams, B.W. Torque ripple analysis and reduction for wind energy conversion systems using uncontrolled rectifier and boost converter. *IET Renew. Power Gener.* **2011**, *5*, 377–386. [[CrossRef](#)]
50. Parker, M.A.; Soraghan, C.; Giles, A. Comparison of power electronics lifetime between vertical- and horizontal-axis wind turbines. *IET Renew. Power Gener.* **2016**, *10*, 679–686. [[CrossRef](#)]
51. Khan, D.; Ahmed Ansari, J.; Aziz Khan, S.; Abrar, U. Power Optimization Control Scheme for Doubly Fed Induction Generator Used in Wind Turbine Generators. *Inventions* **2020**, *5*, 40. [[CrossRef](#)]
52. Zhang, L.; Ren, X.; Ruan, X. A Bandpass Filter Incorporated Into the Inductor Current Feedback Path for Improving Dynamic Performance of the Front-End DC–DC Converter in Two-Stage Inverter. *IEEE Trans. Ind. Electron.* **2014**, *61*, 2316–2325. [[CrossRef](#)]
53. Zhong, Q.; Ming, W.; Cao, X.; Krstic, M. Control of Ripple Eliminators to Improve the Power Quality of DC Systems and Reduce the Usage of Electrolytic Capacitors. *IEEE Access* **2016**, *4*, 2177–2187. [[CrossRef](#)]
54. Shagerdmootaab, A.; Moallem, M. Filter Capacitor Minimization in a Flyback LED Driver Considering Input Current Harmonics and Light Flicker Characteristics. *IEEE Trans. Power Electron.* **2015**, *30*, 4467–4476. [[CrossRef](#)]

55. He, J.; Ruan, X.; Zhang, L. Adaptive Voltage Control for Bidirectional Converter in Flicker-Free Electrolytic Capacitor-Less AC–DC LED Driver. *IEEE Trans. Ind. Electron.* **2017**, *64*, 320–324. [[CrossRef](#)]
56. Krein, P.T.; Balog, R.S.; Mirjafari, M. Minimum Energy and Capacitance Requirements for Single-Phase Inverters and Rectifiers Using a Ripple Port. *IEEE Trans. Power Electron.* **2012**, *27*, 4690–4698. [[CrossRef](#)]
57. Falck, J.; Felgemacher, C.; Rojko, A.; Liserre, M.; Zacharias, P. Reliability of Power Electronic Systems: An Industry Perspective. *IEEE Ind. Electron. Mag.* **2018**, *12*, 24–35. [[CrossRef](#)]
58. Balog, R.; Krein, P.T. Automatic tuning of coupled inductor filters. In Proceedings of the 2002 IEEE 33rd Annual IEEE Power Electronics Specialists Conference. Proceedings (Cat. No.02CH37289), Cairns, Australia, 23–27 June 2002; Volume 2, pp. 591–596.
59. Ale Ahmad, A.; Abrishamifar, A.; Samadi, S. Low-frequency current ripple reduction in front-end boost converter with single-phase inverter load. *IET Power Electron.* **2012**, *5*, 1676–1683. [[CrossRef](#)]
60. Chen, R.; Liu, Y.; Peng, F.Z. DC Capacitor-Less Inverter for Single-Phase Power Conversion With Minimum Voltage and Current Stress. *IEEE Trans. Power Electron.* **2015**, *30*, 5499–5507. [[CrossRef](#)]
61. Chen, W.; Hui, S.Y.R. Elimination of an Electrolytic Capacitor in AC/DC Light-Emitting Diode (LED) Driver With High Input Power Factor and Constant Output Current. *IEEE Trans. Power Electron.* **2012**, *27*, 1598–1607. [[CrossRef](#)]
62. Bose, B.K.; Kastha, D. Electrolytic capacitor elimination in power electronic system by high frequency active filter. In Proceedings of the Conference Record of the 1991 IEEE Industry Applications Society Annual Meeting, Dearborn, MI, USA, 28 September–4 October 1991; Volume 1, pp. 869–878.
63. Zhang, Y.; Jin, K. A single-stage electrolytic capacitor-less AC/DC LED driver. In Proceedings of the 2014 International Power Electronics and Application Conference and Exposition, Shanghai, China, 5–8 November 2014; pp. 881–886.
64. Ohnuma, Y.; Orikawa, K.; Itoh, J. A Single-Phase Current-Source PV Inverter With Power Decoupling Capability Using an Active Buffer. *IEEE Trans. Ind. Appl.* **2015**, *51*, 531–538. [[CrossRef](#)]
65. Ge, B.; Liu, Y.; Abu-Rub, H.; Balog, R.S.; Peng, F.Z.; Sun, H.; Li, X. An Active Filter Method to Eliminate DC-Side Low-Frequency Power for a Single-Phase Quasi-Z-Source Inverter. *IEEE Trans. Ind. Electron.* **2016**, *63*, 4838–4848. [[CrossRef](#)]
66. Chen, M.; Afridi, K.K.; Perreault, D.J. Stacked switched capacitor energy buffer architecture. In Proceedings of the 2012 Twenty-Seventh Annual IEEE Applied Power Electronics Conference and Exposition (APEC), Orlando, FL, USA, 5–9 February 2012; pp. 1404–1413.
67. Afridi, K.K.; Chen, M.; Perreault, D.J. Enhanced Bipolar Stacked Switched Capacitor Energy Buffers. *IEEE Trans. Ind. Appl.* **2014**, *50*, 1141–1149. [[CrossRef](#)]
68. Cao, X.; Zhong, Q.; Ming, W. Ripple Eliminator to Smooth DC-Bus Voltage and Reduce the Total Capacitance Required. *IEEE Trans. Ind. Electron.* **2015**, *62*, 2224–2235. [[CrossRef](#)]
69. Li, S.; Zhu, G.; Tan, S.; Hui, S.Y. Direct AC/DC Rectifier With Mitigated Low-Frequency Ripple Through Inductor-Current Waveform Control. *IEEE Trans. Power Electron.* **2015**, *30*, 4336–4348. [[CrossRef](#)]
70. Wang, H.; Chung, H.S.; Liu, W. Use of a Series Voltage Compensator for Reduction of the DC-Link Capacitance in a Capacitor-Supported System. *IEEE Trans. Power Electron.* **2014**, *29*, 1163–1175. [[CrossRef](#)]
71. Wang, Y.; Wai, R. Adaptive Power Decoupling Strategy for Single-Phase Grid-Connected Converter. *IEEE Trans. Ind. Appl.* **2019**, *55*, 4275–4285. [[CrossRef](#)]
72. Altin, N.; Ozdemir, S.; Komurcugil, H.; Sefa, I. Sliding-mode control in natural frame with reduced number of sensors for three-phase grid-tied LCL-interfaced inverters. *IEEE Trans. Ind. Electron.* **2018**, *66*, 2903–2913. [[CrossRef](#)]
73. Guo, B.; Su, M.; Sun, Y.; Wang, H.; Dan, H.; Tang, Z.; Cheng, B. A robust second-order sliding mode control for single-phase photovoltaic grid-connected voltage source inverter. *IEEE Access* **2019**, *7*, 53202–53212. [[CrossRef](#)]
74. Hollweg, G.V.; Dias de Oliveira Evald, P.J.; Milbradt, D.M.C.; Tambara, R.V.; Gründling, H.A. Lyapunov stability analysis of discrete-time robust adaptive super-twisting sliding mode controller. *Int. J. Control* **2021**, 1–14. [[CrossRef](#)]
75. Hollweg, G.V.; de Oliveira Evald, P.J.D.; Milbradt, D.M.C.; Tambara, R.V.; Gründling, H.A. Design of continuous-time model reference adaptive and super-twisting sliding mode controller. *Math. Comput. Simul.* **2022**, *201*, 215–238. [[CrossRef](#)]
76. Hollweg, G.V.; de Oliveira Evald, P.J.D.; Mattos, E.; Tambara, R.V.; Gründling, H.A. Feasibility Assessment of Adaptive Sliding Mode Controllers for Grid-Tied Inverters with LCL Filter. *J. Control. Autom. Electr. Syst.* **2022**, *33*, 434–447. [[CrossRef](#)]
77. Teng, Q.; Xu, G.; Zheng, X.; Mai, H.; Ma, X.; Wang, Y. A novel sliding mode observer-based compound sliding mode current control with active damping for single phase grid-tied inverter system in weak grid. *Int. J. Electr. Power Energy Syst.* **2022**, *141*, 108117. [[CrossRef](#)]
78. Zhang, X.; Ruan, X.; Kim, H.; Tse, C.K. Adaptive Active Capacitor Converter for Improving Stability of Cascaded DC Power Supply System. *IEEE Trans. Power Electron.* **2013**, *28*, 1807–1816. [[CrossRef](#)]
79. Shimizu, T.; Jin, Y.; Kimura, G. DC ripple current reduction on a single-phase PWM voltage-source rectifier. *IEEE Trans. Ind. Appl.* **2000**, *36*, 1419–1429. [[CrossRef](#)]
80. Mellincovsky, M.; Yuhimenko, V.; Peretz, M.M.; Kuperman, A. Analysis and Control of Direct Voltage Regulated Active DC-Link Capacitance Reduction Circuit. *IEEE Trans. Power Electron.* **2018**, *33*, 6318–6332. [[CrossRef](#)]
81. Nguyen, H.V.; Lee, D. Single-phase multifunctional onboard battery chargers with active power decoupling capability. In Proceedings of the 2018 IEEE Applied Power Electronics Conference and Exposition (APEC), San Antonio, TX, USA, 4–8 March 2018; pp. 3434–3439.

82. Kong, Z.; Huang, X.; Wang, Z.; Xiong, J.; Zhang, K. Active Power Decoupling for Submodules of a Modular Multilevel Converter. *IEEE Trans. Power Electron.* **2018**, *33*, 125–136. [\[CrossRef\]](#)
83. Ansari, J.A.; Liu, C.; Khan, S.A. MMC Based MTDC Grids: A Detailed Review on Issues and Challenges for Operation, Control and Protection Schemes. *IEEE Access* **2020**, *8*, 168154–168165. [\[CrossRef\]](#)
84. Xia, Y.; Roy, J.; Ayyanar, R. A Capacitance-Minimized, Doubly Grounded Transformer less Photovoltaic Inverter With Inherent Active-Power Decoupling. *IEEE Trans. Power Electron.* **2017**, *32*, 5188–5201. [\[CrossRef\]](#)
85. Ohnuma, Y.; Itoh, J. A Novel Single-Phase Buck PFC AC–DC Converter With Power Decoupling Capability Using an Active Buffer. *IEEE Trans. Ind. Appl.* **2014**, *50*, 1905–1914. [\[CrossRef\]](#)
86. Xiao, S.; Li, X.; Zhang, H.; Balog, R.S. Active power decoupling method based on dual buck circuit with model predictive control. In Proceedings of the 2018 IEEE Applied Power Electronics Conference and Exposition (APEC), San Antonio, TX, USA, 4–8 March 2018; pp. 3089–3094.
87. Zhu, G.; Wang, H.; Liang, B.; Tan, S.; Jiang, J. Enhanced Single-Phase Full-Bridge Inverter With Minimal Low-Frequency Current Ripple. *IEEE Trans. Ind. Electron.* **2016**, *63*, 937–943. [\[CrossRef\]](#)
88. Serban, I. Power Decoupling Method for Single-Phase H-Bridge Inverters With No Additional Power Electronics. *IEEE Trans. Ind. Electron.* **2015**, *62*, 4805–4813. [\[CrossRef\]](#)
89. Jamatia, A.; Gautam, V.; Sensarma, P. Power Decoupling for Single-Phase PV System Using Ćuk Derived Microinverter. *IEEE Trans. Ind. Appl.* **2018**, *54*, 3586–3595. [\[CrossRef\]](#)
90. Lyu, X.; Li, Y.; Ni, Z.; Cao, D. A minimized DC-bus capacitor with active combinational decoupling method for DC-AC application. In Proceedings of the 2017 IEEE Applied Power Electronics Conference and Exposition (APEC), Tampa, FL, USA, 26–30 March 2017; pp. 2239–2244.
91. Takaoka, N.; Takahashi, H.; Itoh, J. Isolated Single-Phase Matrix Converter Using Center-Tapped Transformer for Power Decoupling Capability. *IEEE Trans. Ind. Appl.* **2018**, *54*, 1523–1531. [\[CrossRef\]](#)
92. Cai, W.; Jiang, L.; Liu, B.; Duan, S.; Zou, C. A Power Decoupling Method Based on Four-Switch Three-Port DC/DC/AC Converter in DC Microgrid. *IEEE Trans. Ind. Appl.* **2015**, *51*, 336–343. [\[CrossRef\]](#)
93. Tang, Y.; Qin, Z.; Blaabjerg, F.; Loh, P.C. A Dual Voltage Control Strategy for Single-Phase PWM Converters With Power Decoupling Function. *IEEE Trans. Power Electron.* **2015**, *30*, 7060–7071. [\[CrossRef\]](#)
94. Yao, W.; Loh, P.C.; Tang, Y.; Wang, X.; Zhang, X.; Blaabjerg, F. A Robust DC-Split-Capacitor Power Decoupling Scheme for Single-Phase Converter. *IEEE Trans. Power Electron.* **2017**, *32*, 8419–8433. [\[CrossRef\]](#)
95. Shi, Y.; Liu, B.; Duan, S. Low-Frequency Input Current Ripple Reduction Based on Load Current Feedforward in a Two-Stage Single-Phase Inverter. *IEEE Trans. Power Electron.* **2016**, *31*, 7972–7985. [\[CrossRef\]](#)
96. Shimizu, T.; Wada, K.; Nakamura, N. Flyback-Type Single-Phase Utility Interactive Inverter With Power Pulsation Decoupling on the DC Input for an AC Photovoltaic Module System. *IEEE Trans. Power Electron.* **2006**, *21*, 1264–1272. [\[CrossRef\]](#)
97. Hirao, T.; Shimizu, T.; Ishikawa, M.; Yasui, K. A modified modulation control of a single-phase inverter with enhanced power decoupling for a photovoltaic AC module. In Proceedings of the 2005 European Conference on Power Electronics and Applications, Dresden, Germany, 11–14 September 2005; p. 10.
98. Tan, G.H.; Wang, J.Z.; Ji, Y.C. Soft-switching flyback inverter with enhanced power decoupling for photovoltaic applications. *IET Electr. Power Appl.* **2007**, *1*, 264–274. [\[CrossRef\]](#)
99. Yang, Y.; Ruan, X.; Zhang, L.; He, J.; Ye, Z. Feed-Forward Scheme for an Electrolytic Capacitor-Less AC/DC LED Driver to Reduce Output Current Ripple. *IEEE Trans. Power Electron.* **2014**, *29*, 5508–5517. [\[CrossRef\]](#)
100. Wei, Z.; Deng, X.; Gong, C.; Chen, J.; Zhang, F. A novel technique of low frequency input current ripple reduction in two-stage DC-AC inverter. In Proceedings of the IECON 2012—38th Annual Conference on IEEE Industrial Electronics Society, Montreal, QC, Canada, 25–28 October 2012; pp. 139–143.
101. Zhu, G.; Ruan, X.; Zhang, L.; Wang, X. On the Reduction of Second Harmonic Current and Improvement of Dynamic Response for Two-Stage Single-Phase Inverter. *IEEE Trans. Power Electron.* **2015**, *30*, 1028–1041. [\[CrossRef\]](#)
102. Zhang, L.; Ruan, X.; Ren, X. Second Harmonic Current Reduction for Two-Stage Inverter With Boost-Derived Front End Converter: Control Schemes and Design Considerations. *IEEE Trans. Power Electron.* **2018**, *33*, 6361–6378. [\[CrossRef\]](#)
103. Peng, F.Z. Z-source inverter. *IEEE Trans. Ind. Appl.* **2003**, *39*, 504–510. [\[CrossRef\]](#)
104. Liu, Y.; Ge, B.; Abu-Rub, H.; Peng, F.Z. Overview of Space Vector Modulations for Three-Phase Z-Source/Quasi-Z-Source Inverters. *IEEE Trans. Power Electron.* **2014**, *29*, 2098–2108. [\[CrossRef\]](#)
105. Li, Y.; Anderson, J.; Peng, F.Z.; Liu, D. Quasi-Z-Source Inverter for Photovoltaic Power Generation Systems. In Proceedings of the 2009 Twenty-Fourth Annual IEEE Applied Power Electronics Conference and Exposition, Washington, DC, USA, 15–19 February 2009; pp. 918–924.
106. Khan, S.A.; Chongru Liu, C.; Ansari, J.A. Centralized Fuzzy Logic Based Optimization of PI Controllers for VSC Control in MTDC Network. *J. Electr. Eng. Technol.* **2020**, *15*, 2577–2585. [\[CrossRef\]](#)
107. Nguyen, M.; Lim, Y.; Kim, Y. A Modified Single-Phase Quasi-Z-Source AC–AC Converter. *IEEE Trans. Power Electron.* **2012**, *27*, 201–210. [\[CrossRef\]](#)
108. Sun, D.; Ge, B.; Yan, X.; Bi, D.; Zhang, H.; Liu, Y.; Abu-Rub, H.; Ben-Brahim, L.; Peng, F.Z. Modeling, Impedance Design, and Efficiency Analysis of Quasi-Z Source Module in Cascaded Multilevel Photovoltaic Power System. *IEEE Trans. Ind. Electron.* **2014**, *61*, 6108–6117. [\[CrossRef\]](#)

109. Guo, F.; Fu, L.; Lin, C.; Li, C.; Choi, W.; Wang, J. Development of an 85-kW Bidirectional Quasi-Z-Source Inverter With DC-Link Feed-Forward Compensation for Electric Vehicle Applications. *IEEE Trans. Power Electron.* **2013**, *28*, 5477–5488. [[CrossRef](#)]
110. Zhou, Y.; Liu, L.; Li, H. A High-Performance Photovoltaic Module-Integrated Converter (MIC) Based on Cascaded Quasi-Z-Source Inverters (qZSI) Using eGaN FETs. *IEEE Trans. Power Electron.* **2013**, *28*, 2727–2738. [[CrossRef](#)]
111. Rajakaruna, S.; Jayawickrama, L. Steady-State Analysis and Designing Impedance Network of Z-Source Inverters. *IEEE Trans. Ind. Electron.* **2010**, *57*, 2483–2491. [[CrossRef](#)]
112. Yu, Y.; Zhang, Q.; Liu, X.; Cui, S. DC-link voltage ripple analysis and impedance network design of single-phase Z-source inverter. In Proceedings of the 2011 14th European Conference on Power Electronics and Applications, Birmingham, UK, 30 August–1 September 2011; pp. 1–10.
113. Gajanayake, C.J.; Lin, L.F.; Beng, G.H.; Lam, S.P.; Kian, S.L. Extended boost Z-source inverters. In Proceedings of the 2009 IEEE Energy Conversion Congress and Exposition, San Jose, CA, USA, 20–24 September 2009; pp. 3845–3852. [[CrossRef](#)]
114. Qian, W.; Peng, F.Z.; Cha, H. Trans-Z-Source Inverters. *IEEE Trans. Power Electron.* **2011**, *26*, 3453–3463. [[CrossRef](#)]
115. Mo, W.; Loh, P.C.; Blaabjerg, F. Asymmetrical  $\Gamma$ -Source Inverters. *IEEE Trans. Ind. Electron.* **2014**, *61*, 637–647. [[CrossRef](#)]
116. Nguyen, M.; Lim, Y.; Park, S. Improved Trans-Z-Source Inverter With Continuous Input Current and Boost Inversion Capability. *IEEE Trans. Power Electron.* **2013**, *28*, 4500–4510. [[CrossRef](#)]
117. Nguyen, M.; Lim, Y.; Park, S. A Comparison Between Single-Phase Quasi-Z-Source and Quasi-Switched Boost Inverters. *IEEE Trans. Ind. Electron.* **2015**, *62*, 6336–6344. [[CrossRef](#)]
118. Adda, R.; Ray, O.; Mishra, S.K.; Joshi, A. Synchronous-Reference-Frame-Based Control of Switched Boost Inverter for Standalone DC Nanogrid Applications. *IEEE Trans. Power Electron.* **2013**, *28*, 1219–1233. [[CrossRef](#)]
119. Nag, S.S.; Mishra, S. Current-Fed Switched Inverter. *IEEE Trans. Ind. Electron.* **2014**, *61*, 4680–4690. [[CrossRef](#)]
120. Chaturvedi, S.; Fulwani, D.M. Second Order Ripple Reduction in Switched Boost Inverter For Standalone Nanogrid Applications. In Proceedings of the 2019 IEEE 4th International Future Energy Electronics Conference (IFEEEC), Singapore, 25–28 November 2019; pp. 1–6. [[CrossRef](#)]
121. Nguyen, M.; Le, T.; Park, S.; Lim, Y. A Class of Quasi-Switched Boost Inverters. *IEEE Trans. Ind. Electron.* **2015**, *62*, 1526–1536. [[CrossRef](#)]
122. Mishra, S.; Adda, R.; Joshi, A. Inverse Watkins–Johnson Topology-Based Inverter. *IEEE Trans. Power Electron.* **2012**, *27*, 1066–1070. [[CrossRef](#)]
123. Zhang, Y.; Liu, J.; Li, X.; Ma, X.; Zhou, S.; Wang, H.; Liu, Y. An Improved PWM Strategy for Z-Source Inverter With Maximum Boost Capability and Minimum Switching Frequency. *IEEE Trans. Power Electron.* **2018**, *33*, 606–628. [[CrossRef](#)]
124. Abdelhakim, A.; Davari, P.; Blaabjerg, F.; Mattavelli, P. An improved modulation strategy for the three-phase Z-source inverters (ZSIs). In Proceedings of the 2017 IEEE Energy Conversion Congress and Exposition (ECCE), Cincinnati, OH, USA, 1–5 October 2017; pp. 4237–4243.
125. Liu, Y.; Ge, B.; Abu-Rub, H.; Sun, H. Hybrid Pulsewidth Modulated Single-Phase Quasi-Z-Source Grid-Tie Photovoltaic Power System. *IEEE Trans. Ind. Inform.* **2016**, *12*, 621–632. [[CrossRef](#)]
126. Ravindranath, A.; Mishra, S.K.; Joshi, A. Analysis and PWM Control of Switched Boost Inverter. *IEEE Trans. Ind. Electron.* **2013**, *60*, 5593–5602. [[CrossRef](#)]
127. Kachhwaha, M.; Chaturvedi, S.; Fulwani, D. Integral Sliding Mode Control to Compensate Parametric Asymmetry and Modeling Errors in Z-Source Converter. In Proceedings of the 2021 IEEE Industry Applications Society Annual Meeting (IAS), Virtual, 10–14 October 2021; pp. 1–6. [[CrossRef](#)]
128. Kachhwaha, M.; Chaturvedi, S.; Fulwani, D. Parametric Uncertainty Compensation and Ripple Mitigation Control for Family of Z-converters. *IEEE Trans. Ind. Appl.* **2022**, *58*, 7827–7837. [[CrossRef](#)]
129. Chaturvedi, S.; Fulwani, D. Control of Single Stage Inverters and Second-Order Ripple Regulation Using Sliding Mode Control. In *Emerging Trends in Sliding Mode Control: Theory and Application*; Mehta, A., Bandyopadhyay, B., Eds.; Springer: Singapore, 2021; pp. 305–324. [[CrossRef](#)]
130. Yu, Y.; Zhang, Q.; Liang, B.; Cui, S. Single-phase Z-Source inverter: Analysis and Low-frequency Harmonics Elimination Pulse Width Modulation. In Proceedings of the 2011 IEEE Energy Conversion Congress and Exposition, Phoenix, AZ, USA, 17–22 September 2011; pp. 2260–2267.
131. Shen, M.; Wang, J.; Joseph, A.; Peng, F.Z.; Tolbert, L.M.; Adams, D.J. Constant boost control of the Z-source inverter to minimize current ripple and voltage stress. *IEEE Trans. Ind. Appl.* **2006**, *42*, 770–778. [[CrossRef](#)]
132. Nguyen, M.; Tran, T.; Lim, Y. A Family of PWM Control Strategies for Single-Phase Quasi-Switched-Boost Inverter. *IEEE Trans. Power Electron.* **2019**, *34*, 1458–1469. [[CrossRef](#)]
133. Jiang, W.; Wang, Y.; Wang, J.; Wang, L.; Huang, H. Maximizing Instantaneous Active Power Capability for PWM Rectifier Under Unbalanced Grid Voltage Dips Considering the Limitation of Phase Current. *IEEE Trans. Ind. Electron.* **2016**, *63*, 5998–6009. [[CrossRef](#)]
134. Zhang, Y.; Qu, C. Table-Based Direct Power Control for Three-Phase AC/DC Converters Under Unbalanced Grid Voltages. *IEEE Trans. Power Electron.* **2015**, *30*, 7090–7099. [[CrossRef](#)]
135. Song, T.; Wang, P.; Zhang, Y.; Gao, F.; Tang, Y.; Pholboon, S. Suppression Method of Current Harmonic for Three-Phase PWM Rectifier in EV Charging System. *IEEE Trans. Veh. Technol.* **2020**, *69*, 9634–9642. [[CrossRef](#)]

136. Ma, K.; Chen, W.; Liserre, M.; Blaabjerg, F. Power Controllability of a Three-Phase Converter With an Unbalanced AC Source. *IEEE Trans. Power Electron.* **2015**, *30*, 1591–1604. [[CrossRef](#)]
137. Jin, N.; Hu, S.; Gan, C.; Ling, Z. Finite States Model Predictive Control for Fault-Tolerant Operation of a Three-Phase Bidirectional AC/DC Converter Under Unbalanced Grid Voltages. *IEEE Trans. Ind. Electron.* **2018**, *65*, 819–829. [[CrossRef](#)]
138. Sun, D.; Wang, X. Low-complexity model predictive direct power control for DFIG under both balanced and unbalanced grid conditions. *IEEE Trans. Ind. Electron.* **2016**, *63*, 5186–5196. [[CrossRef](#)]
139. Zhang, X.; Li, M.; Xu, D. PCC Voltage Perturbation Path Analysis and Compensation for Grid-Connected Voltage-Source Converter Under Weak Grid. *IEEE Trans. Ind. Electron.* **2021**, *68*, 12331–12339. [[CrossRef](#)]
140. Nian, H.; Liao, Y.; Li, M.; Sun, D.; Xu, Y.; Hu, B. Impedance Modeling and Stability Analysis of Three-Phase Four-Leg Grid-Connected Inverter Considering Zero-Sequence. *IEEE Access* **2021**, *9*, 83676–83687. [[CrossRef](#)]
141. Li, Y.; Du, Z. Stabilizing Condition of Grid-Connected VSC as Affected by Phase Locked Loop (PLL). *IEEE Trans. Power Deliv.* **2022**, *37*, 1336–1339. [[CrossRef](#)]
142. Thanh, V.V.; Su, W.; Wang, B. Optimal DC Microgrid Operation with Model Predictive Control-Based Voltage-Dependent Demand Response and Optimal Battery Dispatch. *Energies* **2022**, *15*, 2140. [[CrossRef](#)]
143. Khan, S.A.; Liu, C.; Ansari, J.A. Unified voltage droop control strategy for VSC-MTDC in HVDC system. In Proceedings of the 16th IET International Conference on AC and DC Power Transmission (ACDC 2020), Online, 2–3 July 2020; Volume 2020, pp. 846–851. [[CrossRef](#)]
144. Su, W.; Wang, J. Energy Management Systems in Microgrid Operations. *Electr. J.* **2012**, *25*, 45–60. [[CrossRef](#)]
145. Tsikalakis, A.G.; Hatziaargyriou, N.D. Centralized Control for Optimizing Microgrids Operation. *IEEE Trans. Energy Convers.* **2008**, *23*, 241–248. [[CrossRef](#)]
146. Kim, J.; Jeon, J.; Kim, S.; Cho, C.; Park, J.H.; Kim, H.; Nam, K. Cooperative Control Strategy of Energy Storage System and Microsources for Stabilizing the Microgrid during Islanded Operation. *IEEE Trans. Power Electron.* **2010**, *25*, 3037–3048.
147. Niyato, D.; Xiao, L.; Wang, P. Machine-to-machine communications for home energy management system in smart grid. *IEEE Commun. Mag.* **2011**, *49*, 53–59. [[CrossRef](#)]
148. Meng, L.; Dragicevic, T.; Guerrero, J.; Vasquez, J.; Savaghebi, M.; Tang, F. Agent-based distributed unbalance compensation for optimal power quality in islanded microgrids. In Proceedings of the 2014 IEEE 23rd International Symposium on Industrial Electronics (ISIE), Istanbul, Turkey, 1–4 June 2014; pp. 2535–2540.
149. McArthur, S.D.J.; Davidson, E.M.; Catterson, V.M.; Dimeas, A.L.; Hatziaargyriou, N.D.; Ponci, F.; Funabashi, T. Multi-Agent Systems for Power Engineering Applications—Part II: Technologies, Standards, and Tools for Building Multi-agent Systems. *IEEE Trans. Power Syst.* **2007**, *22*, 1753–1759. [[CrossRef](#)]
150. Katiraei, F.; Iravani, R.; Hatziaargyriou, N.; Dimeas, A. Microgrids management. *IEEE Power Energy Mag.* **2008**, *6*, 54–65. [[CrossRef](#)]
151. Nasirian, V.; Davoudi, A.; Lewis, F.L. Distributed adaptive droop control for DC microgrids. In Proceedings of the 2014 IEEE Applied Power Electronics Conference and Exposition—APEC 2014, Fort Worth, TX, USA, 16–20 March 2014; pp. 1147–1152. [[CrossRef](#)]
152. Khan, S.A.; Ansari, J.A.; Chandio, R.H.; Munir, H.M.; Alharbi, M.; Alkuhayli, A. AI based controller optimization for VSC-MTDC grids. *Front. Energy Res.* **2022**, *10*, 1008099. [[CrossRef](#)]
153. Dragičević, T.; Lu, X.; Vasquez, J.C.; Guerrero, J.M. DC Microgrids—Part I: A Review of Control Strategies and Stabilization Techniques. *IEEE Trans. Power Electron.* **2016**, *31*, 4876–4891.
154. Dragičević, T.; Lu, X.; Vasquez, J.C.; Guerrero, J.M. DC Microgrids—Part II: A Review of Power Architectures, Applications, and Standardization Issues. *IEEE Trans. Power Electron.* **2016**, *31*, 3528–3549. [[CrossRef](#)]
155. Rajagopalan, J.; Xing, K.; Guo, Y.; Lee, F.C.; Manners, B. Modeling and dynamic analysis of paralleled DC/DC converters with master-slave current sharing control. In Proceedings of the Applied Power Electronics Conference. APEC '96, San Jose, CA, USA, 3–7 March 1996; Volume 2, pp. 678–684.
156. Wu, T.-F.; Chen, Y.-K.; Huang, Y.-H. 3C strategy for inverters in parallel operation achieving an equal current distribution. *IEEE Trans. Ind. Electron.* **2000**, *47*, 273–281.
157. Meng, L.; Dragicevic, T.; Vasquez, J.C.; Guerrero, J.M. Tertiary and Secondary Control Levels for Efficiency Optimization and System Damping in Droop Controlled DC–DC Converters. *IEEE Trans. Smart Grid* **2015**, *6*, 2615–2626. [[CrossRef](#)]
158. Farasat, M.; Mehraeen, S.; Arabali, A.; Trzynadlowski, A. GA-based optimal power flow for microgrids with DC distribution network. In Proceedings of the 2015 IEEE Energy Conversion Congress and Exposition (ECCE), Montreal, QC, Canada, 20–24 September 2015; pp. 3372–3379.
159. Feng, X.; Butler-Purry, K.L.; Zourtos, T. Multi-Agent System-Based Real-Time Load Management for All-Electric Ship Power Systems in DC Zone Level. *IEEE Trans. Power Syst.* **2012**, *27*, 1719–1728. [[CrossRef](#)]
160. Sun, K.; Zhang, L.; Xing, Y.; Guerrero, J.M. A Distributed Control Strategy Based on DC Bus Signaling for Modular Photovoltaic Generation Systems With Battery Energy Storage. *IEEE Trans. Power Electron.* **2011**, *26*, 3032–3045. [[CrossRef](#)]
161. Gu, Y.; Xiang, X.; Li, W.; He, X. Mode-Adaptive Decentralized Control for Renewable DC Microgrid With Enhanced Reliability and Flexibility. *IEEE Trans. Power Electron.* **2014**, *29*, 5072–5080. [[CrossRef](#)]
162. Lu, X.; Guerrero, J.M.; Sun, K.; Vasquez, J.C. An Improved Droop Control Method for DC Microgrids Based on Low Bandwidth Communication With DC Bus Voltage Restoration and Enhanced Current Sharing Accuracy. *IEEE Trans. Power Electron.* **2014**, *29*, 1800–1812. [[CrossRef](#)]

163. Moayedi, S.; Nasirian, V.; Lewis, F.L.; Davoudi, A. Team-Oriented Load Sharing in Parallel DC–DC Converters. *IEEE Trans. Ind. Appl.* **2015**, *51*, 479–490. [[CrossRef](#)]
164. Dam, D.; Lee, H. A Power Distributed Control Method for Proportional Load Power Sharing and Bus Voltage Restoration in a DC Microgrid. *IEEE Trans. Ind. Appl.* **2018**, *54*, 3616–3625. [[CrossRef](#)]
165. Shafiee, Q.; Vasquez, J.C.; Guerrero, J.M. Distributed secondary control for islanded MicroGrids—A networked control systems approach. In Proceedings of the IECON 2012—38th Annual Conference on IEEE Industrial Electronics Society, Montreal, QC, Canada, 25–28 October 2012; pp. 5637–5642.
166. Schiffer, J.; Seel, T.; Raisch, J.; Sezi, T. Voltage Stability and Reactive Power Sharing in Inverter-Based Microgrids With Consensus-Based Distributed Voltage Control. *IEEE Trans. Control Syst. Technol.* **2016**, *24*, 96–109. [[CrossRef](#)]
167. Simpson-Porco, J.W.; Shafiee, Q.; Dörfler, F.; Vasquez, J.C.; Guerrero, J.M.; Bullo, F. Secondary Frequency and Voltage Control of Islanded Microgrids via Distributed Averaging. *IEEE Trans. Ind. Electron.* **2015**, *62*, 7025–7038. [[CrossRef](#)]
168. Tucci, M.; Rivero, S.; Ferrari-Trecate, G. Line-Independent Plug-and-Play Controllers for Voltage Stabilization in DC Microgrids. *IEEE Trans. Control Syst. Technol.* **2018**, *26*, 1115–1123. [[CrossRef](#)]
169. Li, G.-Y.; Zhou, M.; He, J.; Li, G.; Liang, H. Power flow calculation of power systems incorporating VSC-HVDC. In Proceedings of the 2004 International Conference on Power System Technology, 2004. PowerCon 2004, Singapore, 21–24 November 2004; Volume 2, 1562–1566.
170. Zhang, X.-P. Multiterminal voltage-sourced converter-based HVDC models for power flow analysis. *IEEE Trans. Power Syst.* **2004**, *19*, 1877–1884. [[CrossRef](#)]
171. Li, C.; Chaudhary, S.K.; Vasquez, J.C.; Guerrero, J.M. Power flow analysis for droop controlled LV hybrid AC-DC microgrids with virtual impedance. In Proceedings of the 2014 IEEE PES General Meeting | Conference Exposition, National Harbor, MD, USA, 27–31 July 2014; pp. 1–4.
172. Haileselassie, T.M.; Uhlen, K. Impact of DC Line Voltage Drops on Power Flow of MTDC Using Droop Control. *IEEE Trans. Power Syst.* **2012**, *27*, 1441–1449. [[CrossRef](#)]
173. Palma-Behnke, R.; Benavides, C.; Lanas, F.; Severino, B.; Reyes, L.; Llanos, J.; Sáez, D. A Microgrid Energy Management System Based on the Rolling Horizon Strategy. *IEEE Trans. Smart Grid* **2013**, *4*, 996–1006. [[CrossRef](#)]
174. Vaccaro, A.; Popov, M.; Villacci, D.; Terzija, V. An Integrated Framework for Smart Microgrids Modeling, Monitoring, Control, Communication, and Verification. *Proc. IEEE* **2011**, *99*, 119–132. [[CrossRef](#)]
175. Mondal, A.; Misra, S.; Obaidat, M.S. Distributed Home Energy Management System With Storage in Smart Grid Using Game Theory. *IEEE Syst. J.* **2017**, *11*, 1857–1866. [[CrossRef](#)]
176. Shi, W.; Xie, X.; Chu, C.; Gadh, R. Distributed Optimal Energy Management in Microgrids. *IEEE Trans. Smart Grid* **2015**, *6*, 1137–1146. [[CrossRef](#)]
177. Khan, S.A.; Wang, M.; Su, W.; Liu, G.; Chaturvedi, S. Grid-Forming Converters for Stability Issues in Future Power Grids. *Energies* **2022**, *15*, 4937. [[CrossRef](#)]
178. Chang, F.; Cui, X.; Wang, M.; Su, W. Region of Attraction Estimation for DC Microgrids With Constant Power Loads Using Potential Theory. *IEEE Trans. Smart Grid* **2021**, *12*, 3793–3808. [[CrossRef](#)]
179. Hamzeh, M.; Ghazanfari, A.; Mohamed, Y.A.I.; Karimi, Y. Modeling and Design of an Oscillatory Current-Sharing Control Strategy in DC Microgrids. *IEEE Trans. Ind. Electron.* **2015**, *62*, 6647–6657. [[CrossRef](#)]
180. Chaturvedi, S.; Fulwani, D.; Patel, D. Dynamic Virtual Impedance-Based Second-Order Ripple Regulation in DC Microgrids. *IEEE J. Emerg. Sel. Top. Power Electron.* **2022**, *10*, 1075–1083. [[CrossRef](#)]
181. Liu, G.; Caldognetto, T.; Mattavelli, P.; Magnone, P. Suppression of Second-Order Harmonic Current for Droop-Controlled Distributed Energy Resource Converters in DC Microgrids. *IEEE Trans. Ind. Electron.* **2020**, *67*, 358–368. [[CrossRef](#)]
182. Hamzeh, M.; Ghafouri, M.; Karimi, H.; Sheshyekani, K.; Guerrero, J.M. Power Oscillations Damping in DC Microgrids. *IEEE Trans. Energy Convers.* **2016**, *31*, 970–980. [[CrossRef](#)]
183. Chaturvedi, S.; Fulwani, D.; Guerrero, J.M. Adaptive-SMC Based Output Impedance Shaping in DC Microgrids Affected by Inverter Loads. *IEEE Trans. Sustain. Energy* **2020**, *11*, 2940–2949. [[CrossRef](#)]

**Disclaimer/Publisher’s Note:** The statements, opinions and data contained in all publications are solely those of the individual author(s) and contributor(s) and not of MDPI and/or the editor(s). MDPI and/or the editor(s) disclaim responsibility for any injury to people or property resulting from any ideas, methods, instructions or products referred to in the content.